

openAMUNDSEN v1.0: an open source snow-hydrological model for mountain regions

Ulrich Strasser¹, Michael Warscher¹, Erwin Rottler¹ and Florian Hanzer^{1,2}

¹ Department of Geography, University of Innsbruck, Innrain 52, 6020 Innsbruck, Austria

² lumiosys GmbH, Innrain 52, 6020 Innsbruck, Austria

Correspondence: Ulrich Strasser (ulrich.strasser@uibk.ac.at)

Abstract. openAMUNDSEN (= the open source version of the Alpine MULTiscale Numerical Distributed Simulation ENgine) is a fully distributed snow-hydrological model, designed primarily for calculating the seasonal evolution of a snow cover and melt rates in mountain regions. It resolves the mass and energy balance of snow covered surfaces and layers of the snowpack, thereby including the most important processes that are relevant in complex mountain topography. The potential model applications are very versatile; typically, it is applied in areas ranging from the point scale to the regional scale (i.e., up to some thousands of square kilometers), using a spatial resolution of 10–1000 m and a temporal resolution of 1–3 h, or daily. Temporal horizons may vary between single events and climate change scenarios. The openAMUNDSEN model has been applied for many applications already which are referenced herein. It features a spatial interpolation of meteorological observations, several layers of snow with different density and liquid water content, wind-induced lateral redistribution, snow-canopy interaction, glacier ice response to climate, and more. The model can be configured according to each specific application case. A basic consideration for its development was to include a variety of process descriptions of different complexity to set up individual model runs which best match a compromise between physical detail, transferability, simplicity as well as computational performance for a certain region in the European Alps, typically a (preferably gauged) hydrological catchment. The Python model code and example data are available as open source project on GitHub (<https://github.com/openamundsen/openamundsen>; last access: June 1, 2024).

Copyright statement. TEXT

1 Introduction

The seasonal evolution of the mountain snow cover has a significant impact on the water regime, the microclimate and the ecology of mountain catchments and the downstream river regions (Viviroli et al., 2020; Mott et al., 2023). Snow dominated regions are hence crucial for their inhabitants with their function of collecting, storing, and releasing water resources: more than one sixth of the earth's population is relying on seasonal snowpacks (and glaciers) for their water supply (Barnett et al., 2005).

The quantification and prediction of snowmelt amount and dynamics is a challenging task since the complex processes of accumulation, re-distribution and ablation of snow lead to a high variability of the water amount distribution in the mountain snow cover, both in space and time (Viviroli et al., 2007). This high variability challenges both the measuring and modelling of the height and of the water amount of snow (Vionnet et al., 2022), but the understanding of the consequences of climate change on the hydrological effects of a changing mountain snow cover requires an accurate representation of all related processes (Hanzer et al., 2018). Relevant expected changes imply all kind of consequences in the water supply for public and private sectors including hydropower generation, agriculture, forestry and domestic use. Snow processes thereby operate on a variety of spatial and temporal scales (Blöschl, 1999). Further challenges for the modelling of snow processes in mountain regions are imposed by the presence of a forest canopy (Essery et al., 2009; Rutter et al., 2009) which is expected to adapt to the changing climatic conditions and, hence, alter its hydrological effects on the melt rates and the runoff regime from forested mountain regions (Strasser et al., 2011). Finally, the mountain snow cover is an important seasonal landscape feature for all kind of winter touristic activities (Hanzer et al., 2020).

Several types of models with various complexity have been developed to predict the accumulation and ablation of the mountain snow cover (for an overview see Mott et al., 2023). Conceptual models mostly rely on temperature as a proxy for melt rates; their parameters are usually fitted to given streamflow observations (Seibert and Bergström, 2022). Such calibrated temperature index models can provide quite accurate results, since temperature is a physically meaningful replacement of the important energy sources at the snow surface (Ohmura, 2001).

hat gelöscht: 0.8.3

Feldfunktion geändert

Formatiert: Zentriert

hat gelöscht: beneath

hat gelöscht: such regions

hat gelöscht: fold

hat gelöscht: for the public

hat gelöscht: January

hat formatiert: Schriftart: 10 Pt.

Feldfunktion geändert

hat gelöscht: the

hat gelöscht: and also the downstream regions

hat gelöscht: downstream

hat gelöscht: in

hat gelöscht: in mountain regions

hat gelöscht: are

hat gelöscht: of streamflow

64 Furthermore, temperature is a mostly available observation and comparably handy to be interpolated between local
65 recordings. This type of model has been extended with further elements contributing to the energy balance of the
66 snow surface in various form. E.g., Pellicciotti et al. (2005) included potential solar radiation and parameterized
67 albedo of the snow surface into the modelling, allowing for sub-daily time steps of the calculations.

hat gelöscht: and

68 The most sophisticated type of snow models solves the energy balance of the snow surface, requiring a more or
69 less complex description of the short- and longwave radiative fluxes, the turbulent fluxes of sensible and latent
70 heat, the advective heat flux supplied by solid or liquid precipitation and the soil heat flux at the lower boundary
71 of the snow pack. To solve the energy balance equation, these models divide the snowpack into several layers and
72 iteratively compute the state variables for each single layer, usually including respective snow height, density,
73 liquid water content and temperature (e.g., Vionnet et al., 2012; Lehning et al., 1999; Essery, 2015). Sophisticated
74 model concepts of this type also include methods for the correction of the effect of atmospheric stability on the
75 turbulent fluxes (e.g., Sauter et al., 2020).

76 For distributed snow model applications in complex mountain terrain, shadowing of the solar radiation beam and
77 – depending on the application and the considered scale – lateral snow redistribution processes like blowing snow
78 or snow slides should be considered in the modeling, especially if simulations are conducted for longer time
79 horizons (e.g., Vionnet et al., 2021; Quéno et al., 2023). Distributed model applications also require sophisticated
80 methods for the spatial interpolation of the local meteorological station recordings (see, e.g., MeteolO; Bavay and
81 Egger, 2014), or downscaling procedures to utilize gridded weather or climate model output to force the
82 simulations.

Feldfunktion geändert

83 Very recently, methods of artificial intelligence have undergone a hype-like push for development of new
84 modelling approaches: these make use of the forcing variables governing any processes changing a system, and
85 time series of observations of its state. In a certain perspective these models are similar to calibrated models, with
86 empiricism thereby replaced by statistics. However, the same limitations exist for such statistical approaches like
87 for the empirical ones in terms of transferability of their application in space and time. First attempts also exist to
88 complement complex physical snow models with data-driven machine learning approaches, e.g. the “Deep
89 Learning national scale 1 km resolution snow water equivalent (SWE) prediction model“
90 (<https://github.com/whitelightning450/SWEML>; last access: June 1, 2024). Similar developments are undertaken
91 in the field of weather forecasting (e.g., Lam et al., 2023), with respective implications on the predictability of the
92 snow cover evolution. It can be expected that in this domain many innovations will emerge in the near future.

hat gelöscht: January

Feldfunktion geändert

93 Most of the sophisticated energy balance snow (hydrological) models which are currently in development are
94 available as open source projects, e.g. Surfex (<https://www.umr-cnrm.fr/surfex>; last access: June 1, 2024), CRHM
95 (<https://github.com/CentreForHydrology/CRHM>; last access: June 1, 2024), FSM
96 (<https://github.com/RichardEssery/FSM>; last access: June 1, 2024), SNOWPACK (<https://snowpack.slf.ch>; last
97 access: June 1, 2024), COSIPY (<https://github.com/cryotools/cosipy>; last access: June 1, 2024), or, as described
98 in the following, openAMUNDSEN (<https://github.com/openamundsen/openamundsen>; last access: June 1, 2024).

hat gelöscht: for the public

hat gelöscht: such as

hat gelöscht: ,

hat gelöscht: January

Feldfunktion geändert

hat gelöscht: January

Feldfunktion geändert

Feldfunktion geändert

hat gelöscht: January

Feldfunktion geändert

hat gelöscht: January

hat gelöscht: January

Feldfunktion geändert

hat gelöscht: January

Feldfunktion geändert

hat gelöscht:

hat gelöscht: 0.9

hat gelöscht: lapse rate

hat gelöscht: scheme

hat gelöscht: ,

hat gelöscht: if necessary

99 openAMUNDSEN v1.0, the snow-hydrological model described herein, comprises many of the presented snow
100 model principles, from simple empirical approaches to coupled energy and mass balance calculations. The model
101 mainly is built upon a comprehensive, physically based description of snow processes typical for high mountain
102 regions. In particular, the main features of the model include:

- 103 • Spatial interpolation of scattered meteorological point measurements considering elevation using a combined
104 regression/inverse distance weighting (IDW) procedure
- 105 • Calculation of solar radiation taking into account terrain slope and orientation, hillshading and atmospheric
106 transmission losses as well as gains due to scattering, absorption, and multiple reflections between the snow
107 surface and clouds
- 108 • Adjustment of precipitation using several correction functions for wind-induced undercatch and lateral
109 redistribution of snow using terrain-based parameterizations
- 110 • Simulation of the snow and ice mass and energy balance using either a multi-layer scheme or a bulk scheme
111 using four separate layers for new snow, old snow, firn and ice
- 112 • Alternatively, a temperature index/enhanced temperature index method, the latter considering potential solar
113 radiation and albedo of the surface
- 114 • Usage of arbitrary timesteps (e.g. 10 minutes, hourly, or daily) while resampling of forcing data to the desired
115 temporal resolution.
- 116 • Flexible output of time series including arbitrary model variables for selected point locations in NetCDF or
117 CSV format

- Flexible output of gridded model variables, either for specific dates or periodically (e.g. daily or monthly), optionally aggregated to averages or totals in NetCDF, GeoTIFF or ASCII grid format
- Built-in generation of future meteorological data time series as model forcing with a given trend using a bootstrapping algorithm for the available historical time series of the meteorological recordings
- Live view window for the visualization of selectable variables of the model state during runtime.

hat gelöscht: ,

hat gelöscht: illustrating

Together with the model, a comprehensive set of data that can be used to run the model for the upper Rofental (Ötztal Alps/Austria, 98.1 km²) is available at Pangaea (<https://doi.org/10.1594/PANGAEA.876120>; last access: June 1, 2024) (Strasser et al., 2018) and at <https://doi.org/10.5880/figeo.2023.037> (not active yet; temporarily it is <https://dataservices.gfz-potsdam.de/panmetanetworks/review/3671cf380a6c433e48f5ec5a4cfa1179dd88c1af297665405aaa139e7b77c24a/>; last access: June 1, 2024. See also Warscher et al., 2024). Further, an openAMUNSEN example setup is available at GitHub (<https://github.com/openamundsen/openamundsen-examples>; last access: June 1, 2024). This data can be used to setup and run the model for this catchment and to conduct a multitude of simulation experiments like sensitivity tests and evaluation; it can also serve as example to be replaced by data from other catchments or sites. The Rofental is used also in the following as demonstration site to illustrate the functionalities of the model.

hat gelöscht: Tyrol

Feldfunktion geändert

hat gelöscht: January

hat gelöscht: as well as in form of

hat gelöscht: on

hat gelöscht: January

Feldfunktion geändert

hat gelöscht: freely

hat gelöscht: .

hat gelöscht: This data

hat gelöscht: example

2 Model evolution

The AMUNSEN model has a development history of well over twenty years. Originally, the model was prepared to compute fields of meteorological variables, snow albedo and melt with a new enhanced temperature index approach (Pellicciotti et al., 2005). Later, a simple surface energy balance method based on ESCIMO¹ (Strasser and Mauser, 2001) was integrated. The model was then applied and continuously improved to simulate snow hydrological variables for Haut Glacier d'Arolla (Strasser et al., 2004) and the high alpine region of the Berchtesgaden National Park (Strasser, 2008). Strasser et al. (2008) investigated the sublimation losses of the alpine snow cover from the ground and vegetated surfaces, as well as during blowing snow events. In Strasser et al. (2011), snow-canopy processes were modelled for a chess-board pattern of various forest stands and open areas on an idealized mountain. The simple bulk energy balance core of the model also exists as a spread-sheet based point scale scheme where only hourly meteorological variables have to be pasted in to run the snow simulations for a particular observation site (Strasser and Marke, 2010). This spread-sheet based model was later extended by the snow-canopy interaction processes that were already implemented in AMUNSEN (Marke et al., 2016). The energy balance approach was continuously further developed, e.g. with an iterative procedure to account for atmospheric stability (after Weber, 2008) or with the introduction of a 4-layer scheme (new snow, old snow, firn, glacier ice; Hanzer et al., 2016). Hanzer et al. (2014) developed a module for the production of technical snow on skiing slopes. Historical and future snow conditions for Austria were determined with the model by Marke et al. (2015) and Marke et al. (2018), respectively. Hanzer et al. (2016) presented a parameterization for lateral snow redistribution based on topographic openness, and multi-level spatiotemporal validation as a systematic, independent, complete and redundant validation procedure. The hydrological response and glacier evolution in a changing climate was investigated by Hanzer et al. (2018) for the Ötztal Alps in Austria. Modelled SWE also provided a reference for the fusion with satellite-data derived snow distribution maps in a machine learning framework (De Gregorio et al., 2019a and b), or to determine distributed glacier mass balance (Podsiadlo et al., 2020). Pfeiffer et al. (2021) used the model to compute the amount of liquid water provided for infiltration by snowmelt and rainfall for determining conditions that fostered the motion of a landslide in the Tyrolean Alps. With the transition to the open source project openAMUNSEN, the multi-layer approach by Essery (2015) was integrated into the model as further alternative to compute the mass and energy balance of a layered snow pack. Finally, the openAMUNSEN model has been used to simulate the entire process of snow management and snow conditions for the slopes in skiing areas (Hanzer et al., 2020, Ebner et al., 2021).

hat gelöscht: , respectively

hat gelöscht: determine

The first distributed version of the AMUNSEN model was developed in IDL (= Interactive Data Language, see <https://www.nv5geospatialsoftware.com/Products/IDL>; last access: June 1, 2024), originally documented in Strasser (2008) and – in a more recent evolutionary stage – in Hanzer et al. (2018). Recently, the model code was completely re-programmed in Python and transferred into an open source project (<https://github.com/openamundsen/openamundsen>; last access: June 1, 2024); this was the moment when the model was renamed to “openAMUNSEN”. An online documentation is currently in production

hat gelöscht: January

Feldfunktion geändert

hat gelöscht: January

Feldfunktion geändert

¹ The first point-scale version of the snow model was named Energy balance Snow Cover Integrated Model (“ESCIMO”) and programmed in Fortran (Strasser and Mauser, 2001). Later, when the first distributed version was developed in IDL, it was renamed to “AMUNSEN” (Strasser et al., 2004).

200 (<https://doc.openamundsen.org>; last access: June 1, 2024). New developments which are not yet available online
 201 in the GitHub repository will be published there after comprehensive testing.

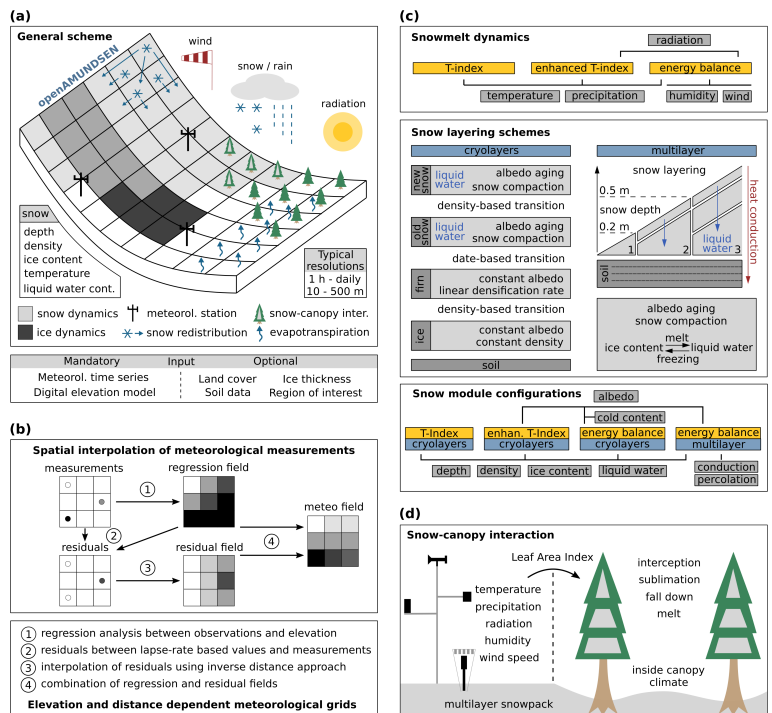
hat gelöscht: January
 Feldfunktion geändert

202 3 Model concept

203 3.1 General structural design

204 The fundamental principles and most important capabilities of the model are shown in the general overview (figure
 205 1a). The region for which openAMUNDSEN is to be set up is a rectangle comprised by a digital elevation model
 206 (DEM) in raster format. This DEM defines the extent and resolution for which the model computations are
 207 performed. The model is capable to simulate the mass balance of both snow and/or glacier ice surfaces, as well as
 208 lateral redistribution of snow, snow-canopy interaction and evapotranspiration from different land cover types.
 209 Irregular observations of meteorological stations or gridded output from any kind of raster model are distributed
 210 over the domain by means of an IDW procedure considering dependence on elevation in each timestep and
 211 spatially interpolated local residuals of the recordings (figure 1b): alternatively, fix monthly gradients can be
 212 applied. Several approaches of varying complexity are available to compute surface melt, from a simple
 213 temperature-index method over an enhanced index approach considering temperature, potential solar radiation and
 214 albedo to sophisticated energy balance methods (figure 1c). These melt approaches can be combined with two
 215 layering schemes in a total of four different snow model configurations. Each of these configurations can be
 216 applied to forest conditions, where a modified set of the meteorological variables is provided to account for the
 217 effect of the trees on the inside-canopy microclimatic conditions, parameterized by means of the Leaf Area Index
 218 (LAI) as the variable describing the characteristics of the forest (figure 1d).

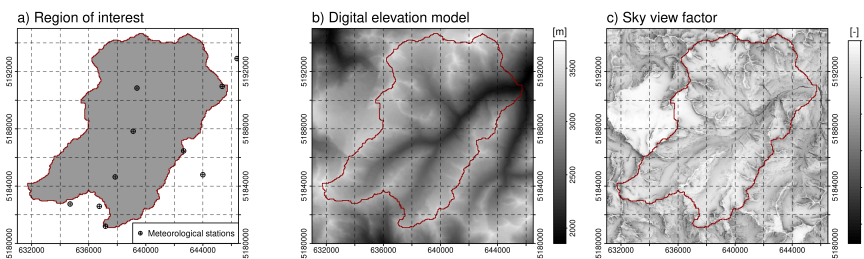
hat gelöscht: combined inverse distance procedure
 hat gelöscht: an
 hat gelöscht: elevation gradient(e.g., the lapse rate
 hat gelöscht: of temperature)
 hat gelöscht: different
 hat gelöscht: e



219
 220 Figure 1: Schematic representation of a domain modelled with the snow-hydrological model openAMUNDSEN
 221 (a), spatial interpolation of the meteorological measurements (b), snowmelt dynamics and snow layering schemes
 222 and (c) and scaling of observed to inside-canopy meteorological conditions for the simulation of snow-canopy
 223 interaction processes (d) in the model.

231 To save computational time, it is possible to define an irregular region of interest (ROI; i.e., a sub-quantity of
 232 pixels); outside this area only some required calculations for the interpolation of the meteorological variables will
 233 be computed (figure 2a). Typically, a ROI is a watershed area for which water balance components are aggregated
 234 from the single pixel values, so that resulting streamflow volume can be compared to gauge recordings (Hanzer et
 235 al., 2018). Weather stations to be considered can also be located outside the ROI, or even outside the DEM area;
 236 however, in the latter case they cannot be considered for the determination of shadow areas or regional-scale
 237 albedo which is used to estimate the diffuse radiative fluxes by multiple scattering between the surface and the
 238 atmosphere. Extent and resolution of the DEM defines the cell size and the geometry of all other raster layers
 239 produced in the simulations (figure 2b). From this DEM, several derived variables such as slope, aspect and sky
 240 view factor are calculated (figure 2c). The sky view factor is the ratio of the visible sky that can be seen from a
 241 pixel location to the entire hemisphere that contains both visible and obstructed sky.

hat gelöscht: ,
 hat gelöscht: and
 hat gelöscht: ,
 hat gelöscht: and
 hat gelöscht: portion of the visible sky, i.e. the



242
 243 Figure 2: Region of interest (ROI) of the openAMUNDSEN example application to the Rofental (Ötztal
 244 Alps/Austria) with location of weather stations in- and outside this region of interest (a), digital elevation model
 245 (b) and sky view factor (c). The red line is the watershed divide of the Rofental for the gauge at Vent (1891 m
 246 a.s.l.).

hat gelöscht: Tyrolean
 hat gelöscht: the

247 The meteorological forcing for the simulations typically consists of time series of temperature, relative humidity,
 248 precipitation, global radiation and wind speed. These variables are standard observations at the meteorological
 249 stations of operational weather services and mostly available for many mountain regions (e.g. in Austria:
 250 www.geosphere.at; last access: June 1, 2024). To accurately track the daily course of radiative energy – usually
 251 the most important component of the energy for melt (Strasser et al., 2004) – the time step in the modelling in
 252 most applications is hourly. To save computational time, the model computations can also be limited to 2- or 3-
 253 hourly time steps. If the optional temperature index approach is selected the time step also can be set to daily. For
 254 the case that specific submodules are activated for a model run (e.g., snow-canopy interaction or
 255 evapotranspiration), various other spatial input fields have to be prescribed (e.g., land cover, soil and/or catchment
 256 boundaries).

hat gelöscht: ,
 hat gelöscht: It is also possible to use sub-hourly time steps, . or, t
 hat gelöscht: or, t
 hat gelöscht: ,
 hat gelöscht: if
 hat gelöscht: ,
 hat gelöscht: ,

257 When using meteorological station data as input the minimum number of stations required is one. This station
 258 should provide a continuous series of measurements without gaps. If more than one weather station exists, missing
 259 values at a particular site are replaced by the respective results from the interpolation procedure. Where recordings
 260 exist, the interpolated values might slightly differ due to the difference in altitude between the exact location of
 261 the station and the grid pixel in which it is located (and for which the meteorological field is interpolated).
 262 Alternatively to station recordings, it is also possible to provide pre-processed gridded meteorological fields as
 263 input to the model, e.g. output data from numerical weather prediction or climate models. Data timeseries of future
 264 climate evolution to force openAMUNDSEN for climate change scenario simulations can be produced by means
 265 of a stochastic block bootstrap resampler which is realized as external routine in Python (see Appendix).

hat gelöscht: already
 hat gelöscht: pre-processing
 hat formatiert: Schriftart: 10 Pt., Englisch (USA)

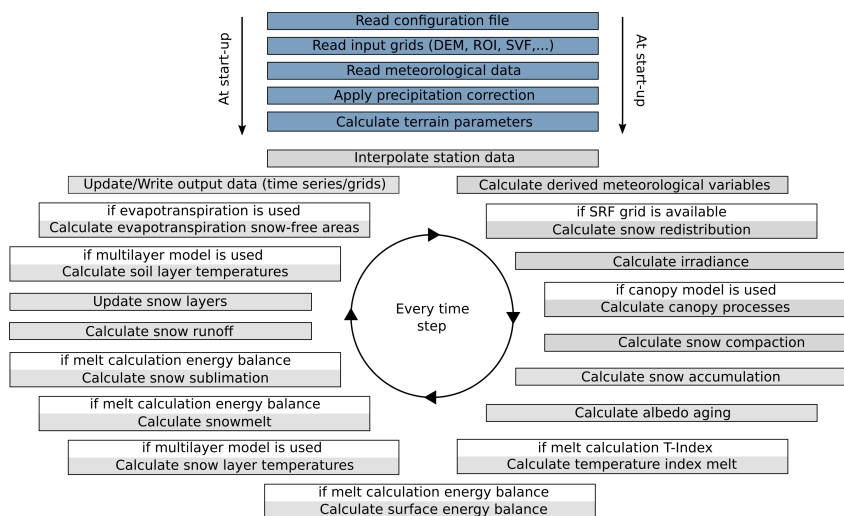
266 The model simulations are performed for each pixel and each timestep (figure 3). Prior to these pixel-wise
 267 computations for the raster domain a set of general computations for the model run are performed: after reading
 268 the input data the terrain parameters are computed from the DEM, and precipitation correction parameters are
 269 computed (as described in 3.5). Then the time-dependent computations for all pixels of the domain start, in a loop
 270 from the first to the last time step of the particular simulation run. Several modules are subject to options which
 271 can be set in a configuration file in text format.

272 The results of the computations can be written to file either as time series for an arbitrary number of pixels (in
 273 NetCDF or CSV format), or as gridded model variables for specific selected dates or periodically (e.g., daily,

291 monthly, or yearly), optionally aggregated to averages or totals. Possible formats include NetCDF, GeoTIFF and
 292 ASCII grid.

293 To keep modelling time to a minimum, state variables (e.g., from a spin-up simulation) can be imported as raster
 294 grids to initialize an openAMUNDSEN model run. Some state variables can also be computed prior to the model
 295 run. E.g., if glacier outlines are available, the initial ice thickness distribution can be calculated using the approach
 296 by Huss and Farinotti (2012). Volumetric balance fluxes of individual glaciers can be calculated from mass balance
 297 gradients and constants. Surface elevations and glacier outlines are usually published in glacier inventories
 298 (<https://wgms.ch>; last access: June 1, 2024), e.g. for Austria in Fischer et al. (2015).

- hat gelöscht: ,
- hat gelöscht: or
- hat gelöscht: spin-up
- hat gelöscht: s
- hat gelöscht: n
- hat gelöscht: acceptable
- hat gelöscht: January
- Feldfunktion geändert



299 Figure 3: Flowchart showing the repetitive circle of a typical openAMUNDSEN model run. The reading of the
 300 input is succeeded by the computation of several precipitation correction and terrain parameters. After that, the
 302 loop for all time steps of the model run is entered.

- hat gelöscht: calculation

303 3.2 Temporal and spatial discretization

304 Usually the model is driven with a temporal resolution according to the one of the used meteorological forcing
 305 variables. For model applications which require a higher temporal resolution (or if only daily recordings are
 306 available) methods exist to disaggregate the measurements accordingly (e.g. MELODIST; Förster et al., 2016).
 307 For simulations with lower temporal resolution than the forcing, aggregation is done during runtime. Output
 308 temporal resolution can be any aggregate of the original computation resolution – usually daily, monthly and
 309 yearly. All this is arbitrarily set in the model configuration prior to the model run. The minimum spatial resolution
 310 is not limited. Theoretically, a 1 m or even higher resolution (e.g. laser-scan derived) DEM can be used as basis
 311 for the model simulation. A comparatively high resolution thereby is beneficial for adequately capturing all small-
 312 scale processes shaping the snow cover distribution in complex terrain. However, it is questionable if such
 313 computational effort is meaningful with respect to the availability and quality of the forcing data and to the scale
 314 of the considered processes. According to our experiences from typical mountain catchments in the European
 315 Alps, a resolution between 10 m and 1000 m is often a good compromise between detail representation and
 316 computational efficiency. The size of the modelled domain can be anything between one single pixel and some
 317 thousands of square kilometers (see figure 1a). De Gregorio et al. (2019a, b), e.g., successfully applied the model
 318 for the Euregio Tyrol/South Tyrol/Trentino (Austria/Italy) which has a size of 26254 km².

- hat gelöscht: ,
- hat gelöscht: Any
- hat gelöscht: hence also
- hat gelöscht: ,
- hat gelöscht: s
- hat gelöscht: several tens of
- hat gelöscht: with

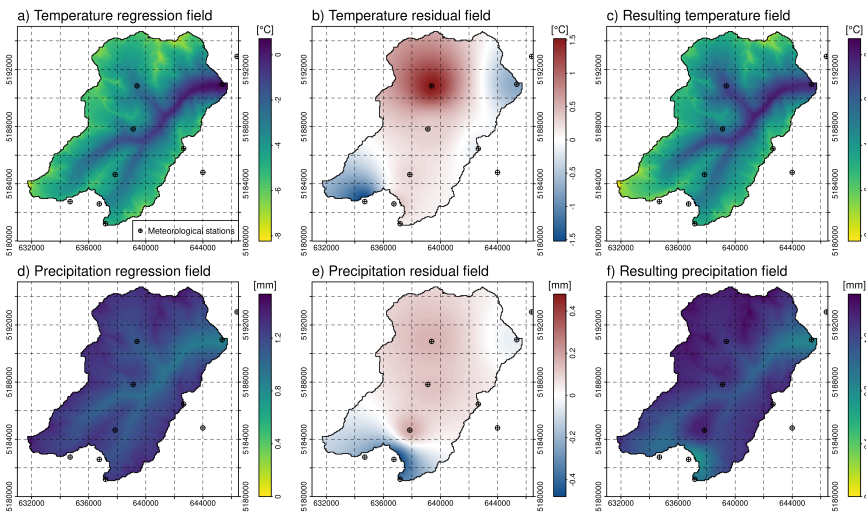
319 3.3 Spatial interpolation of meteorological measurements

320 openAMUNDSEN includes a meteorological pre-processor for the spatial interpolation of scattered point
 321 measurements, irrespective whether these are provided irregularly (weather station recordings) or arranged as a

337 regular grid (raster stack of weather or climate model output). In the latter case, the meteorological variables are
 338 resampled to grids with the given DEM spatial resolution. The minimum forcing required by the model consists
 339 of recordings of temperature and precipitation (when running in temperature index mode). For energy balance
 340 calculations, relative humidity, global radiation (or cloudiness) and wind speed are required in addition. If
 341 meteorological time series from station recordings are used as input, the model interpolates the measurements
 342 from their geographical locations to each grid cell inside the ROI (figure 4). In most simulation cases, recordings
 343 of the meteorological variables for the 2 m observation level are available. The distance between a variable snow
 344 surface and the sensor height can therefore be corrected in the modelling. To spatially interpolate the station
 345 observations in each model time step, the following IDW-based interpolation procedure is applied:

- 346 • a regression analysis between observations and the associated station elevation is performed to derive an
 347 elevation-dependent trend function: the lapse rate (LR),
- 348 • the derived function is applied to all cells of the DEM to create an elevation trend field for each meteorological
 349 variable, the "regression field" (figures 4a and 4d)
- 350 • the residuals for all station locations are calculated by subtracting the calculated regression value for the
 351 station elevation from the actual measurement at the station location for the current time step,
- 352 • the residuals for the station locations are interpolated to the grid using an IDW method, resulting in the
 353 "residual field" (figures 4b and 4e),
- 354 • this interpolated residual field is added to the regression field, which results in elevation- and station distance-
 355 dependent interpolated fields for all meteorological variables (figures 4c and 4f).

356 Figure 4 exemplarily shows the steps of this IDW-based interpolation procedure for temperature and precipitation.
 357 It can be seen that for both meteorological variables a dependency of the recordings with elevation does exist
 358 (figure 4a and 4d), but locally some deviations of the measurements from the elevation trend occur (figure 4b and
 359 4e). In the result both patterns are visible. The procedure automatically fills potential gaps in the observation time
 360 series at the weather station locations. If only one observation for the LR determination exists at a given time step
 361 for the entire domain, this one observed value is uniformly distributed over the domain.



362
 363 Figure 4: Regression field, residual field and the resulting meteorological field, i.e. sum of the two for the spatial
 364 interpolation of meteorological variables in each single time step, exemplarily shown for temperature (a, b and c)
 365 and for precipitation (d, e and f) on 24/12/2019 at 10 am for the Rofental. The resolution of the interpolated grid
 366 is 20 m.

367 Instead of the dynamic LR calculated from the local observations in each time step, the prescribed average monthly
 368 values of MicroMet (Liston and Elder, 2006) can be used. MicroMet is a quasi-physically based meteorological
 369 observation distribution system of intermediate complexity to produce high-resolution atmospheric forcings

hat gelöscht: are

hat gelöscht: as well

hat gelöscht: of

hat gelöscht: only

hat gelöscht: (t

hat gelöscht: for

hat gelöscht:)

hat gelöscht: For

hat gelöscht: each model time step

hat gelöscht: ,

hat gelöscht: (the lapse rate)

hat gelöscht: from

hat gelöscht: (raster cells)

hat gelöscht: inverse distance weighting (

hat gelöscht:)

hat gelöscht: the

hat gelöscht:

hat gelöscht: , respectively

hat gelöscht: temperature and precipitation

hat gelöscht: are considered

hat gelöscht: become

hat gelöscht:

hat gelöscht: is

hat gelöscht:

hat gelöscht: ,

hat gelöscht: e

hat gelöscht: trend

hat gelöscht: IDW

hat gelöscht: in

hat gelöscht: lapse

hat gelöscht: rates

hat gelöscht: point data

hat gelöscht: gradients

hat gelöscht: can be used as well, e.g.

hat gelöscht: following Liston and Elder (2006)

hat gelöscht: -

required to run spatially distributed terrestrial models in complex topography. It distributes the variables air temperature, relative humidity, wind speed, incoming solar (shortwave) and longwave radiation, surface pressure and precipitation following a Barnes objective analysis scheme, similar to the IDW procedure applied in openAMUNDSEN. A detailed comparison of results achieved with the interpolation schemes of openAMUNDSEN, MicroMet (and others, e.g. MeteoIO: Bavay and Egger, 2014) and respective effects on the snow processes modelling would be an interesting task of scientific value, but is beyond the scope of this paper. Here we only demonstrate the dynamic (mostly hourly) derived from the station observations in openAMUNDSEN for the Rofental and their monthly averages compared to the standard temperature LR and monthly values originating from other regional contexts (figure 5): e.g., the monthly average temperature LR derived for the Upper Danube catchment in central Europe are several degrees above the ones derived for the Northern Hemisphere; this shows the necessity of calculating LR using local observations. It should be noted, however, that dynamic temperature LR and their monthly averages may vary from year to year.

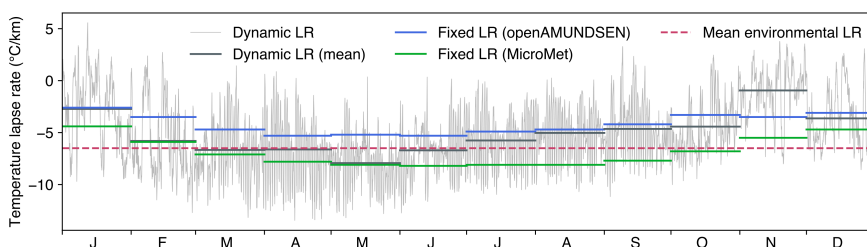


Figure 5: Dynamic (mostly hourly) temperature LR for 2020 in the Rofental (gray). The fixed LR are monthly averages derived for the Upper Danube catchment (blue; Marke, 2008) and the Northern Hemisphere (green; Liston and Elder, 2006). The dashed line shows the mean environmental LR of -6.5 °C km^{-1} . Monthly averages computed for the dynamic LR (derived from the observations in each model time step) are dark grey.

Finally, precipitation phase is determined in openAMUNDSEN by either air temperature or wet-bulb temperature thresholds (wet-bulb temperature is computed by iteratively solving the psychrometric equation). For both methods, a temperature transition range is defined. Above this transition range, precipitation is determined as liquid, and as solid below the lower end of the temperature range, respectively. Within the defined temperature range, the fractions of solid/liquid precipitation are linearly distributed between 100 % liquid at the upper and 100 % solid at the lower end of the range with 50 % liquid/solid fraction of precipitation at the threshold temperature. The threshold used in the presented simulations here was chosen empirically: a value of 0.5 °C wet bulb temperature with a transition extent from 0 °C to 1 °C produced reliable results in many numerical experiments with the model, in particular for the well-gauged site Rofental (see Hanzer et al., 2016).

3.4 Radiative fluxes

Incoming global radiation strongly varies in time and space depending on terrain characteristics, position of the sun and atmospheric conditions. Hence, openAMUNDSEN calculates potential global radiation for each grid cell based on local aspect and slope, position of the sun, orographic shadows, atmospheric transmission losses and gains due to scattering, absorption and reflections, multiple reflections between snow and clouds as well as reflected radiation from snow covered neighbouring slopes. Cloud coverage (when not prescribed) is either determined by comparing potential to observed global radiation; or, alternatively, it is estimated using atmospheric humidity following Liston and Elder (2006). During nighttime either the atmospheric humidity approach is used or cloudiness is kept constant. In the final step, cloud coverage is spatially interpolated and actual incoming global radiation is calculated by correcting potential global radiation with cloud coverage for each model grid cell.

Reflected short wave radiation depends on surface albedo which strongly varies in space and time, for snow surfaces mainly depending on grain size. In openAMUNDSEN, albedo is modelled taking into account snow age and an air temperature-dependent decay function following Rohrer (1992) and Essery et al. (2013):

$$\alpha = \alpha_{\min} + (\alpha_{t-1} - \alpha_{\min}) \cdot e^{-\frac{1}{\tau} \delta t}$$

hat gelöscht: as

hat gelöscht: described above

hat gelöscht: ,

hat gelöscht: (LR)

hat gelöscht: means

hat gelöscht: lapse rates

hat gelöscht: the lapse rates

hat gelöscht: lapse rates

hat gelöscht: .

Formatiert: Zentriert

hat gelöscht: /2021

hat gelöscht: Dynamic temperature lapse rates also vary from year to year.

hat gelöscht: Precipitation

hat formatiert: Schriftart: Nicht Kursiv

hat formatiert: Schriftart: Nicht Kursiv

hat gelöscht: ¶

hat gelöscht: 1

461 where α_{\min} is the (prescribed) minimum albedo, α_{t-1} the albedo in the previous time step, δt the time step length,
 462 and τ is a temperature-dependent recession factor (implemented by prescribing two factors τ_{pos} and τ_{neg} for positive
 463 and negative air or, optionally, surface temperatures). Maximum snow albedo α_{\max} is by default set to 0.85, while
 464 α_{\min} , τ_{pos} , and τ_{neg} are set to 0.55, 200 h, and 480 h. Firm and ice albedo are held constant with $\alpha_{\text{firm}} = 0.4$ and $\alpha_{\text{ice}} =$
 465 0.2 by default. Fresh snow increases albedo, either using a step function – increasing albedo to α_{\max} when a
 466 snowfall above a certain threshold amount per timestep (default: $0.5 \text{ kg m}^{-2} \text{ h}^{-1}$) occurs – or using the continuous
 467 function

468
$$\alpha = \alpha_{t-1} + (\alpha_{\max} - \alpha_{t-1}) \frac{S_f}{S_0},$$

469 where S_f is the snowfall amount and S_0 the snowfall required to refresh albedo (Essery et al., 2013).

470 Incoming longwave radiation from the atmosphere is a function of atmospheric conditions and temperature and is
 471 determined using the Stefan-Boltzmann law. Atmospheric emissivity thereby depends on water vapour content in
 472 clear sky conditions and cloud cover in overcast situations. Additionally, openAMUNDSEN accounts for long-
 473 wave radiation from the neighbouring slopes. Outgoing longwave radiation is calculated following the Stefan-
 474 Boltzmann law with the emissivity of snow and modelled snow surface temperature. The details of the radiation
 475 model mostly follow Corripio (2002) and are described in Strasser et al. (2004).

476 3.5 Precipitation correction

477 Precipitation measurements are vital input for every snow-hydrological model. However, measuring solid
 478 precipitation in complex alpine terrain is prone to large errors which typically results in an undercatch of
 479 precipitation (Rasmussen et al., 2012). This is particularly important for mountain regions with a high amount of
 480 solid precipitation. High wind speeds can cause an undercatch of snowfall up to 50 % (Kochendorfer et al., 2017)
 481 when using typical pluviometers of the Hellmann type. For solid precipitation, different correction methods are
 482 implemented in the model in order to account for the undercatch of precipitation gauges when measuring snow
 483 accumulation. Hanzer et al. (2016) showed that a combination of a weather station-based snow correction factor
 484 taking into account wind speed and air temperature based on an approach by the World Meteorological
 485 Organization (WMO; Goodison et al., 1998) with a subsequent constant post-interpolation additional factor
 486 yielded plausible precipitation amounts. Whereas the first correction is applied for the station recording amount
 487 prior to interpolation to the cells of the rectangular grid, the latter is added to all grid cells of the modelling domain.
 488 Alternatively to the WMO approach, a method which estimates undercatch regardless of precipitation phase
 489 (Kochendorfer et al., 2017) can be selected in the model configuration procedure prior to a model run.

490 3.6 Snow redistribution

491 Irrespective whether rain or snow, with the IDW interpolation scheme in openAMUNDSEN the amount of
 492 precipitation is distributed over the domain depending on the grid cell elevation, the distance of the surrounding
 493 weather stations and the selected gauge undercatch correction method. The amount of observed snow at a certain
 494 location, however, can be significantly affected by the lateral processes of preferential deposition, erosion and
 495 lateral redistribution. These processes are driven by wind and gravitational forces (Warscher et al., 2013;
 496 Grünewald et al., 2014). Many approaches with different complexity exist to account for these processes; a recent
 497 and comprehensive overview of modelling lateral snow redistribution is given by Quéno et al. (2023). Such
 498 consideration of the lateral snow redistribution processes is required to prevent artefacts of continuous snow
 499 accumulation on high summits and crests in long-term simulations where melt during summer is not sufficient to
 500 remove the amount of snow accumulated during the previous winter. The result will be that with increasing
 501 simulation period, in such locations “snow towers” will continuously grow, whereas in depressions beneath snow
 502 accumulation will be underestimated (Freudiger et al., 2017). As a consequence, mass balances of existing glaciers
 503 in such locations will be increasingly wrong due to not enough mass deposited in the accumulation areas. Mass
 504 balances therefore are a useful measure to evaluate the simulations with respect to the lateral snow redistribution
 505 processes, as demonstrated by Hanzer et al. (2016). In openAMUNDSEN a snow redistribution factor (SRF) field
 506 can be used to parameterize spatial snow distribution. The SRF describes the fractional amount of snow either
 507 eroded or deposited at each pixel location and modifies the interpolated snowfall field accordingly. Since SRF
 508 derivation can depend on various topographic parameters such as elevation, slope, aspect, curvature, viewshed or
 509 terrain roughness, and generally requires site-specific calibration (Grünewald et al., 2013), openAMUNDSEN
 510 allows for flexibility in calculating the SRF field. It provides functions to compute these topographic parameters
 511 but does not prescribe a singular method for final SRF calculation. Instead, the user of the model can decide in

hat gelöscht: long-term

hat gelöscht: modified

hat gelöscht: ,

hat nach unten verschoben [1]: Their consideration is a prerequisite for long-term simulation experiments, because – if neglected – the model will overestimate snow accumulation on summits and crests, whereas in the depressions beneath it will be underestimated; as a consequence, also mass balances of existing glaciers in such locations might be wrong due to not enough mass deposited in the accumulation areas.

hat gelöscht: A

hat gelöscht: also

hat gelöscht: ¶

hat gelöscht: (figure

hat gelöscht: 5

hat gelöscht: 6a)

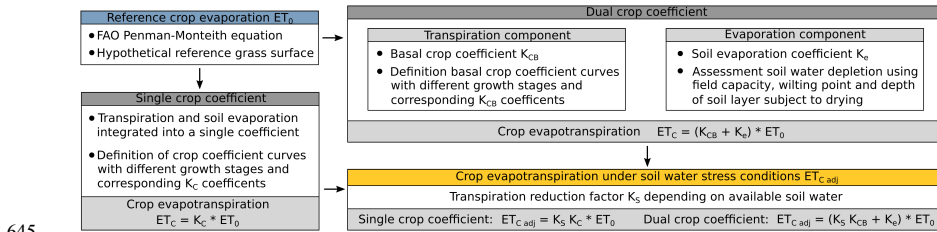
606 the trees composing the stands, i.e. the sum of the classical LAI and the Cortex Area Index CAI (Strasser et al.,
 607 2011). By means of the modified meteorological variables, the processes of interception, sublimation, unloading
 608 by melt and fall down by exceeding the canopy snow-holding capacity are calculated. Liquid precipitation is
 609 assumed to fall through the canopy and is added to the ground snow cover (see figure 1d).

610 Simulations with the snow-canopy interaction model for an idealized mountain (Strasser et al., 2011) showed that,
 611 despite reduced accumulation of snow on the ground beneath the trees, both rates and seasonal totals of sublimation
 612 of snow previously intercepted in a canopy were significantly higher than the sublimation losses from the ground
 613 snow surface. On top of that, shadowing leads to reduced radiative energy input inside the canopy and hence
 614 protection of the snow at the ground. The type of forest, exposition, the specific meteorological conditions and the
 615 general evolution of the winter season play an important role as well: during winter, the effect of reduced
 616 accumulation is dominant, whereas during spring, the shadowing effect with reduced ablation prevails. In winters
 617 with much snow, the effect of shadowing by the trees dominates and snow lasts longer inside the forest than in the
 618 open. In winters with little snow, however, the sublimation losses of snow are dominant and the snow lasts longer
 619 in open areas. This might vary, however, for northern and southern exposure to radiation and time of the year due
 620 to the strong effect of solar radiation on melt. In early and high winter, the radiation protection effect of shadowing
 621 is small. An intermittent melt out of the snow cover beneath the trees can occur if little snow is available. The
 622 shadowing effect becomes more efficient and snowmelt is delayed relative to nonforested areas in late winter and
 623 spring. Due to the combination of all these processes, the modelling of snow-canopy interaction can lead to
 624 complex and very heterogeneous patterns of snow coverage and duration in alpine regions with forest stands
 625 (Essery et al., 2009; Rutter et al., 2009; Strasser et al., 2011).

626 3.8 Crop evapotranspiration

627 For non-snow-covered surfaces the actual evapotranspiration of vegetated areas is calculated using the FAO
 628 Penman-Monteith approach (Allen et al., 1998), for which a schematic overview is illustrated in figure 7. In a first
 629 step, the evapotranspiration is calculated for a reference crop (grass) using the meteorological variables and a
 630 limiting amount of available water in the soil storage. In forested areas, thereby the inside-forest meteorological
 631 conditions are considered. Then, the resulting evapotranspiration is modified according to the vegetation type
 632 using particular crop coefficients which integrate the effects of plant height, albedo, stomata resistance and
 633 exposed soil fraction. Crop coefficients are available for a wide range of plant types in the given literature and
 634 change their value along the season according to predefined growth stage lengths. For each plant type,
 635 evapotranspiration can either be calculated using a single-coefficient approach which integrates the effects of crop
 636 transpiration and soil evaporation into a single coefficient, or using a dual-coefficient approach which considers
 637 crop transpiration and soil evaporation separately. Soil evaporation is computed considering the cumulative depth
 638 of water evaporated from the top soil layer and the fraction of the soil surface that is both exposed and wetted. The
 639 soil type thereby determines the amount of evaporable amount of water with respect to field capacity, water content
 640 at wilting point and depth of the surface soil layer that is subject to drying by means of evaporation (0.10 to 0.15
 641 m); parameters are available for sand, loamy sand, sandy loam, loam, silt loam, silt, silt clay loam silty clay and
 642 clay (Allen et al., 1998). With this approach the water balance of the upper soil layer is computed, determining if
 643 surface runoff and deep percolation can occur or if evapotranspiration is limited. If the evapotranspiration module
 644 is activated, both soil types and land cover must be available as rasterized maps in the DEM geometry.

hat gelöscht: 6



645

646 Figure 7: Schematic overview of the FAO evapotranspiration module to compute the water flux from the soil
 647 through the plants to the atmosphere with the Penman-Monteith equation. Fluxes are calculated for a reference
 648 crop and then scaled to other landuse classes.

hat gelöscht: 6

651 3.9 Layering schemes

652 In openAMUNDSEN two different layering schemes for snow- or ice-covered surfaces are implemented (see
653 figure 1c). The “cryospheric layer version“ parameterizes layers of new snow, old snow, firn and glacier ice. The
654 advantage of using these layers is that they are distinctively different in their optical properties, and hence, their
655 surfaces can be recognized and distinguished in the field, on photographs, or by satellites with sensors sensitive in
656 the visible range of the electromagnetic spectrum. The model tracks the thickness of these layers and parameterizes
657 their density with more or less empirical relations. For the snow-soil interface a fix upwards heat flux can be set
658 (often 2 W m^{-2} in the Alpine region). The most comprehensive descriptions of this model versions can be found
659 in Strasser (2008), Strasser et al. (2011) and Hanzer et al. (2016).

- hat gelöscht: ;
- hat gelöscht: by humans
- hat gelöscht: or
- hat gelöscht: ground
- hat gelöscht: usually

660 The “multi-layer version“ is adopted following the structure of the FSM model (Essery, 2015). It considers a
661 number of layers (by default three) with fixed maximum depths (for the upper two ones), all of them without
662 physical representation. In this model version the fluxes of mass and energy are tracked by means of an iterative
663 computation of the state variables temperature and liquid water content such that the balances of mass and energy
664 are closed for each layer. The energy transfer at the snow-soil interface is calculated by means of a 4-layer soil
665 model. A detailed description of the implemented multi-layer model scheme can be found in Essery (2015).

666 Whereas the cryospheric layer version of openAMUNDSEN can be combined with both the simple or the enhanced
667 temperature-index approach or, alternatively, with the energy balance method, the multi-layer version requires the
668 energy balance method to compute the energy and mass balances of the surface and the snow layers beneath. The
669 simulation of glacier evolution as a response to the climatic conditions presupposes the cryospheric layer version
670 to be applied.

- hat gelöscht: (see figure 1c)
- hat gelöscht: requires
- hat gelöscht: cryolayer version

671 3.9.1 Cryospheric layer version

672 In the cryospheric layer version of openAMUNDSEN, the transitions between new snow and old snow occur when
673 reaching a predefined snow density threshold (by default 200 kg m^{-3}), while remaining snow amounts at the end
674 of the ablation season are transferred to the firn layer (by default on 30 September). Compaction for the new and
675 old snow layers is calculated using the methods described below (in 3.10); for firn a linear densification is assumed.
676 Once reaching a threshold density of 900 kg m^{-3} , firn is added to the ice layer beneath. While snow albedo is
677 parameterized using the aging curve approach (Rohrer, 1992), firn and ice albedo is kept constant (with default
678 values of 0.4 and 0.2, respectively). The details of the cryospheric layer version of openAMUNDSEN are best
679 described in Hanzer et al. (2016).

- hat gelöscht: are transferred to the firn layer

680 While snow temperature of the individual layers is not calculated using the cryospheric layering scheme, an
681 approach following Braun (1984) and Blöschl and Kirnbauer (1991) is applied in order to determine an average
682 cold content of the snow layers. This cold content builds up when the snowpack cools; it has to be depleted before
683 melt and subsequent runoff can occur at the snowpack bottom. The maximum possible cold content is thereby set
684 to 5 % of the total snowpack weight (the latter can be converted to an energy by multiplication with the latent heat
685 of fusion).

686 When using this scheme, the snowpack is taken as a bulk layer to solve the surface energy balance. If air
687 temperature is above 0 °C the model assumes that the snow surface temperature is 0 °C and melt occurs, the
688 amount of which can be computed from the available excess of the energy balance. If the air temperature is below
689 0 °C , an iterative procedure to compute the snow surface temperature for closing the energy balance is applied.
690 With this procedure, the snow surface temperature is altered until the residual energy balance passes zero.

691 3.9.2 Multi-layer version

692 In the multi-layer version of openAMUNDSEN, the vertical heat fluxes are computed through both the snow pack
693 and into the ground (Essery, 2015). To solve the energy balance, melt is first assumed to be zero for the surface
694 temperature change of every timestep. Snow is melting if the energy balance results in a surface temperature
695 passing 0 °C . The temperature increment is recalculated assuming that all of the snow melts; if this results in a
696 surface temperature below 0 °C , snow only partially melts during the timestep (Essery, 2015). Snow layer
697 temperatures are then updated using an implicit finite difference scheme. Snow compaction and density of each
698 layer are calculated in the same way as for the cryospheric layer version, as described in the following.

708 3.10 Snow density

709 For both layering schemes, fresh snow density is calculated using the temperature-dependent parameterization by
710 Anderson (1976), assuming a minimum density of 50 kg m^{-3} . Snow compaction can be calculated using two
711 methods, one physically based approach following Anderson (1976) and Jordan (1991), and one empirical
712 approach following Essery (2015). For the former, density changes are calculated in two stages due to snow
713 compaction and metamorphism, taking into account temperature and snow load imposed by the layers above (see
714 also Koivusalo et al., 2001). For the empirical method, assumptions are made for maximum density of snow below
715 $0 \text{ }^\circ\text{C}$ and for melting conditions (default values: 300 kg m^{-3} for cold snow and 500 kg m^{-3} for melting snow). The
716 timescale for compaction is an adjustable parameter (default value: 200 h). The increase of density for every
717 timestep is calculated as a fraction of the compaction timescale multiplied with the difference of maximum density
718 and the density of the last timestep (Essery, 2015).

719 3.11 Liquid water content

720 Meltwater occurring at the snow surface is not immediately removed from the snowpack, but a certain liquid water
721 content (LWC) can be retained. Following either Braun (1984) or Essery (2015), the maximum LWC is defined
722 as mass fraction of SWE or as a fraction of pore volume that can be filled with liquid water (volumetric water
723 content). If the maximum LWC is reached during snowmelt, runoff at the bottom of a snow layer occurs and drains
724 to the snow layer underneath, or – for the bottom snow layer – into the upper soil layer respectively. In the case of
725 a negative energy balance, this liquid water can refreeze.

726 3.12 Snowmelt

727 Snowmelt can be computed in openAMUNDSEN by several approaches with different complexity. The simplest
728 method, the classical temperature index approach, is particularly suited for regions where only daily recordings of
729 temperature and precipitation are available. Melt M in mm per timestep is thereby computed as:

$$730 \quad M = \begin{cases} \text{DDF} \cdot T & T > T_T \\ 0 & T \leq T_T \end{cases}$$

731 with DDF being the degree day factor (or melt coefficient) in $\text{mm w.e. } ^\circ\text{C day}^{-1}$ and T the mean daily temperature
732 in $^\circ\text{C}$. T_T is the threshold temperature above which melt is assumed to occur (e.g., $1 \text{ }^\circ\text{C}$). Low DDFs will be
733 obtained for cold and dry areas, whereas high DDFs can be expected for warm and wet areas.

734 Second is a hybrid approach between the temperature index method and the energy balance, the so-called
735 "enhanced temperature index method" by Pellicciotti et al. (2005). By including potential shortwave radiation and
736 albedo these computations can be applied to meteorological variables in hourly time steps:

$$737 \quad M = \begin{cases} \text{TF} \cdot T + \text{RF} \cdot (1 - \alpha) \cdot G & T > T_T \\ 0 & T \leq T_T \end{cases}$$

738 where T is an hourly temperature in $^\circ\text{C}$, α is albedo and G is potential incoming shortwave radiation (which is
739 simulated as described in 3.4). TF and RF are two empirical coefficients, the temperature factor and the shortwave
740 radiation factor, expressed in $\text{mm h}^{-1} \text{ }^\circ\text{C}^{-1}$ and $\text{m}^2 \text{ mm W}^{-1} \text{ h}^{-1}$. T_T is equal to $1 \text{ }^\circ\text{C}$. When temperature is below T_T
741 no melt occurs.

742 Melt rates using either the cryospheric layer or the multi-layer version of openAMUNDSEN also can be computed
743 using the surface energy balance equation:

$$744 \quad Q + H + E + A + B + M = 0$$

745 with Q being the shortwave and longwave radiation balance, H the sensible heat flux, E the latent heat flux, A the
746 advective energy supplied by solid or liquid precipitation and B the soil heat flux. M is the energy potentially
747 available for melt. For a detailed description of the calculation of the individual energy fluxes see Strasser (2008).
748 A comparison of modelling results achieved with the different approaches is shown in figure 8. The temperature
749 index approach delivers results which only show dependence on the temperature and the precipitation gradient,
750 but no pattern affected by different radiative energy input depending on slope and aspect (figure 8a). These
751 computations can be performed with daily time step, hence they are comparably fast and only require temperature

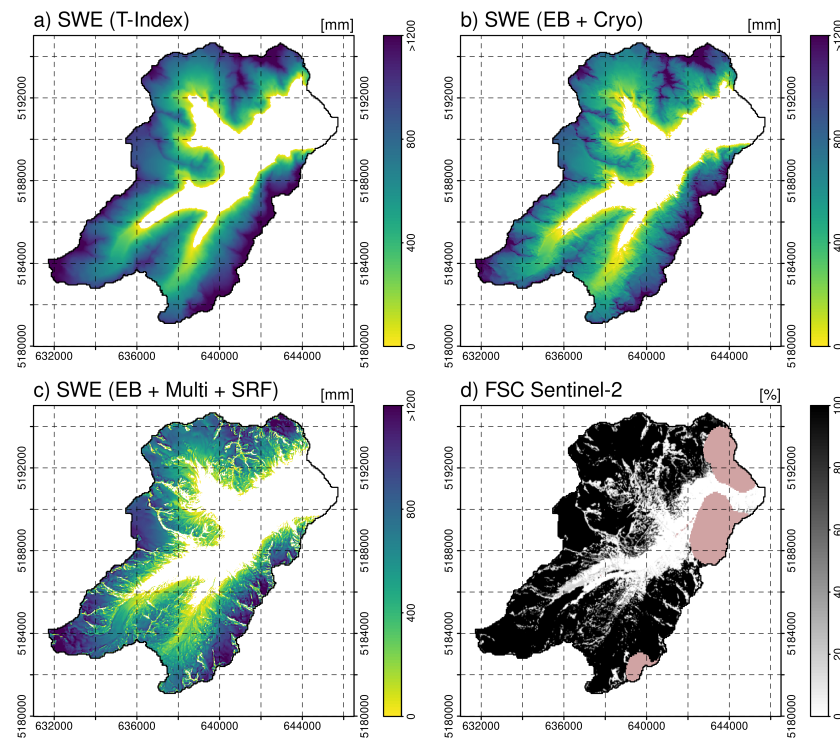
hat gelöscht: S

hat gelöscht: S

hat gelöscht: 7

hat gelöscht: 7a

756 and precipitation as meteorological input variables. Using the energy balance for computation of the accumulation
 757 and ablation processes at the snow surface, and the **cryospheric layer version** for the internal processes inside the
 758 snow pack, leads to a significantly more differentiated pattern of **resulting** snow distribution (figure 8b): The result
 759 clearly shows the effect of topography on the ablation pattern of the snow cover on this day. In figure 8c, the
 760 energy balance was combined with the multi-layer version of the model and the application of the SRF to consider
 761 the lateral snow redistribution processes. Now, erosion from exposed summit and ridge areas can be detected, as
 762 well as additional accumulation in the slopes beneath. This complex pattern best matches the snow distribution as
 763 depicted in the fractional snow cover map derived from a Sentinel-2 image captured on the same day (figure 8d).
 764 **The comparison of the simulation results achieved with increasingly sophisticated model versions shows that their**
 765 **plausibility clearly improves with consideration of radiative energy supply (8b) and lateral snow redistribution**
 766 **(8c).**



767
 768 Figure 8: Snow water equivalent on 18/06/2019 in the Rofental, simulated using the **temperature index** approach
 769 in daily resolution without wind-induced snow redistribution (a), **using** the energy balance (EB) approach and
 770 cryospheric layers (Cryo) without wind-induced snow redistribution (b) **and using** the energy balance (EB)
 771 approach with multi-layers (Multi) including wind-induced snow redistribution (SRF) (c). Panel (d) shows a
 772 fractional snow cover (FSC: including the glacier areas) map **derived from** Sentinel-2 satellite data for the same
 773 day (pink bobbles are unclassified pixels, in this case clouds).

774 **Implementation in Python**

775 For the rewriting of the original AMUNDSEN IDL code the Python language was chosen due to its popularity,
 776 simplicity and the large number of excellent and well-tested numerical and scientific libraries available.
 777 openAMUNDSEN especially makes use of the packages NumPy (Harris et al., 2020) for array calculations, pandas
 778 (McKinney, 2010) and Xarray (Hoyer and Hamman, 2017) for processing time series and multidimensional data
 779 sets. While Python, being a scripting language, has limitations in terms of execution performance, these libraries

hat gelöscht: cryolayer version

hat gelöscht: 7b

hat gelöscht: 7c

hat gelöscht: on this particular day

hat gelöscht: 7d

hat gelöscht: 7

hat gelöscht: 18

hat gelöscht: T-I

hat gelöscht: ,

hat gelöscht: based on

hat gelöscht: .

hat gelöscht: 4 Generation of potential future climate
 Future scenarios of climate can be produced by means of a stochastic "block bootstrap resampler" (Mausser et al., 2007) which is realized in a pre-processing routine for openAMUNDSEN (<https://github.com/openamundsen/openamundsen-climategenerator>; last access January 1, 2024). The method requires a sufficiently long time series of meteorological recordings from a period with highly variable weather conditions in the considered region. The principles of the implemented weather generator follow Strasser (2008) and are described herein. The basic assumption of the method is that a climate storyline can be divided into time periods which are characterized by a certain mean temperature and precipitation and that these two variables are not independent from each other:

$$P_{tot} = f(T_{mean})$$

P_{tot} is the total precipitation amount of a specific time period, T_{mean} is the mean temperature and f their functional dependency. The time periods can be set to any length, i.e. to months as in Mausser et al. (2007) or to weeks as in Strasser (2008). In a first step, the typical annual course of the measured meteorological variables is constructed by computing mean temperature and total precipitation for the periods using all years of the historical dataset and applying the given formula. Whereas temperature is characterized by a typical seasonal course in the Alpine region (warm in summer, cold in winter), the annual course of the precipitation totals of a period with certain duration can be more complex. The resulting mean annual climate course is used to construct the future data time series period by period: firstly, the respective temperature for the period is modified with a random variation factor and an assumed projected trend (e.g., as suggested from a regional climate model). Then a corresponding precipitation is derived and, again, a random variation. In the end the climate of a future period is defined by the so obtained mean temperature and precipitation. In a final step, the period from the historical pool having the most similar temperature and precipitation is selected by applying an Euclidian nearest neighbour distance measure. All respective data of the chosen period (e.g., air temperature, precipitation, global radiation, relative humidity and wind speed) are then added to the future time series to be constructed. This procedure is repeated for all periods of the year, and for all years of the future time series. By modifying the applied random variation a change in climate variability can be simulated. To allow for more flexibility in the construction of the periods, in our implementation the basic population from which the measured period is chosen (= the number of periods available, being equal to the number of years for which observational data is available) can be (... [2])

906 allow efficient code execution due to the use of Fortran or C for the underlying calculations. For increasing the
907 runtime efficiency of performance-critical functions within openAMUNDSEN, the Numba library (Lam et al.,
908 2015) is furthermore used for dynamically translating Python code into machine code.

909 openAMUNDSEN is implemented using an object oriented architecture, centering around the `OpenAmundsen`
910 class as the primary interface. This class represents a single model run and encapsulates all methods required to
911 initialize and run the model. openAMUNDSEN can either be used as a stand-alone utility (using the
912 `openamundsen` command line tool) or as a Python library. When used in stand-alone mode, the
913 `openamundsen` command line tool must be invoked with the name of a configuration file in YAML format (i.e.,
914 `openamundsen config.yml`). If used as a library from within a Python script, the model configuration in
915 form of a Python dictionary (commonly again sourced from a YAML file) must be passed when instantiating an
916 `OpenAmundsen` object. A typical model run executed from within Python looks as follows:

```
917 import openamundsen as oa
918
919 config = oa.read_config('config.yml')
920 model = oa.OpenAmundsen(config)
921 model.initialize()
922 model.run()
```

923 This allows for substantial flexibility in simulation preparation, execution and postprocessing. For example:

- 924 • It is possible to change the model state variables after initializing them (e.g., the snow layers – which are by
925 default initialized as being snow-free – can be initialized using prepared snow depth or SWE data). This is
926 not only possible prior to running the model, but can also be done at any point during the model run by using
927 `model.run_single()` – which performs the calculations for a single time step – in a loop, instead of the
928 `model.run()` call
- 929 • Model results do not necessarily have to be written to file but can also be stored in-memory and accessed
930 directly from the `OpenAmundsen` class instance for further processing
- 931 • Several model runs can be prepared in a single script by initializing multiple `OpenAmundsen` instances and,
932 e.g., be run in parallel.

933 Model runtime is influenced by various factors, most importantly the number of pixels simulated, but also the
934 number of weather stations used for interpolation of the meteorological variables, the choice of the layering scheme
935 (cryospheric layers vs. multi-layer), the activated submodules (snow-canopy interaction, evapotranspiration, etc.),
936 the amount of I/O operations (the number of output variables and the temporal frequency in which they are written
937 to file), and others. openAMUNDSEN generally leverages multiple CPU cores (by operating over the model grid
938 pixels in parallel using Numba's parallelization features), however in practice the speedup gained by parallelism
939 is small due to the short-lived nature of the respective functions and the overhead from scaling to multiple cores.
940 To give an example, a point-scale (i.e., 1x1) model run completes a full-year simulation using hourly time steps
941 in approx. 2 minutes on an AMD EPYC 7502P processor. A spatially distributed model run for a medium-sized
942 model grid (450 x 650 pixels) requires approx. 36 minutes per simulation year in single-core mode, and
943 33/30/28/27 minutes when using 2/4/8/16 cores, respectively. Running the model in pure Python mode (i.e.,
944 disabling the Numba just-in-time compilation) can increase runtime by a factor of more than 40.

945 § Model uncertainty and evaluation

946 The original versions of ESCIMO and then AMUNDSEN have been extensively validated in various Alpine sites
947 (Strasser and Mauser, 2001; Strasser et al., 2002; Strasser, 2004; Pellicciotti et al., 2005; Strasser et al., 2008;
948 Strasser, 2008; Hanzer et al., 2014; Marke et al., 2015). Hanzer et al. (2016) showed the uncertainty of the model
949 application by means of a systematic, independent, complete and redundant validation procedure based on the
950 observation scale of temporal and spatial support, spacing, and extent (Blöschl, 1999). To evaluate the dimensions
951 of the observation scale a comprehensive set of eight independent validation sources was used: (i) mean areal
952 precipitation derived by conserving mass in the closure of the water balance, (ii) time series of snow depth
953 recordings at the plot scale, (iii-iv) multitemporal snow extent maps derived from Landsat and MODIS satellite
954 data products, (v) snow accumulation distribution derived from airborne laser scanning data, (vi) specific surface
955 mass balances for three glaciers in the study area, (vii) spatially distributed glacier surface elevation changes for
956 the entire area and (viii) runoff recordings for several subcatchments. By means of this evaluation procedure, both
957 the simulated spatial patterns of the snow cover, as well as time series of its evolution, are quantitatively analyzed

hat gelöscht: (see also figure 8)

hat gelöscht: (

hat gelöscht:)

hat gelöscht: 6

with a maximum of considered independent comparison measures: the method hence represents an unprecedented completeness in the comparison of the simulation results with observations. The results indicate a high overall model skill in all the dimensions and confirmed the very good model evaluations of the published case studies (Hanzer et al., 2016). As an example for the model performance at the location of a meteorological station, figure 9 shows snow depth (9a) and SWE (9b) simulation results achieved with meteorological observations at the Proviantdepot station (2737 m a.s.l.) compared to recordings of snow depth for the winter seasons 2020/2021 and 2021/2022. All model versions well capture the seasonal course of the snow depth evolution. Of course, the temperature index version could be optimized by means of calibration to better match the meltout time, so the lag of some days is not a lack of model "accuracy" in this case (a standard degree day factor of $6.0 \text{ mm K}^{-1} \text{ d}^{-1}$ was used, the same as for the results in figure 8a, without further calibration). The energy balance version of the model using the multilayer approach and considering lateral snow redistribution provides the best matching representation of the observations.

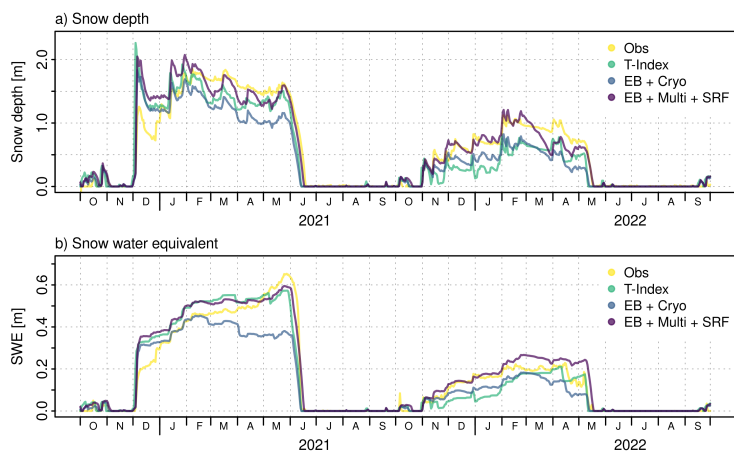


Figure 9: Observed and simulated snow depth (a) and SWE (b) at the location of the meteorological station Proviantdepot (2737 m a.s.l.) located in the area of the example application Rofental (46.82951°N , 10.82407°E) for the winter seasons 2020/2021 and 2021/2022. The Pearson correlation/Nash-Sutcliffe efficiency/Kling-Gupta efficiency/RMSE for the T-index simulations of snow depth is 0.92/0.79/0.77/0.269, and for SWE 0.96/0.93/0.94/0.055. For the EB+Cryo model version, it is 0.93/0.70/0.61/0.283 (snow depth) and 0.94/0.76/0.65/0.076 (SWE), and for the EB+Multi+SRF model simulation 0.96/0.92/0.95/0.186 (snow depth) and 0.98/0.95/0.88/0.046 (SWE), respectively.

For the multi-layer version of the openAMUNDSEN model, the uncertainty of the model simulations was investigated by Günther et al. (2019) for point simulations at the local scale and by Günther et al. (2020) for distributed applications.

openAMUNDSEN was also subject to several model intercomparison studies. The very first version of the bulk energy balance approach of AMUNDSEN (then still called ESCIMO) was compared to CROCUS for data of the Col de Porte weather station located in the French Alps (1340 m a.s.l.) (Strasser et al., 2002). Later, the model was intercompared to many other snow models in the series of the international Snow Model Intercomparison Projects (SnowMIPs): in the original SnowMIP project (Etchevers et al., 2004), ESCIMO was evaluated together with 22 other snow models of varying complexity at the point scale using meteorological observations from the two mountainous Alpine sites Col de Porte (1340 m a.s.l.) and Weissfluhjoch (2540 m a.s.l.), both in the European Alps. In the follow-up project SnowMIP2 (<https://www.geos.ed.ac.uk/~ressery/SnowMIP2.html>; last access: June 1, 2024), thirty-three snowpack models of varying complexity and purpose were evaluated across a wide range of hydrometeorological and forest canopy conditions at five Northern Hemisphere locations, namely (Essery et al., 2009; Rutter et al., 2009): Alptal (Switzerland; 1185 m a.s.l.), BERMS (Canada; 579 m a.s.l.), Fraser (USA; 2820 m a.s.l.), Hitsujigaoka (Japan; 182 m a.s.l.) and Hyytiälä (Finland; 181 m a.s.l.). For each location two sites were used, one in the open (no canopy) and one forested (canopy) site. Finally, the surface energy balance core of the model participated in ESM-SnowMIP (<https://climate-cryosphere.org/esm-snowmip/>; last access: June 1, 2024).

- hat gelöscht: 9
- hat gelöscht: 2019
- hat gelöscht: to
- hat gelöscht: 2020
- hat gelöscht: Despite the missed significant snowfall event at the beginning of the season, all
- hat gelöscht: The
- hat gelöscht: 9
- hat gelöscht: 5
- hat gelöscht: 7a
- hat gelöscht: Both
- hat gelöscht: versions
- hat gelöscht: well
- hat gelöscht: .

- hat gelöscht: 9
- hat formatiert: Englisch (USA)
- hat gelöscht: 2019
- hat gelöscht: 0
- hat formatiert: Englisch (USA)
- hat formatiert: Englisch (USA)
- hat formatiert: Englisch (USA)
- hat formatiert: Englisch (USA)
- hat formatiert: Englisch (USA)
- hat formatiert: Schriftfarbe: Schwarz

- hat gelöscht: January
- Feldfunktion geändert
- hat verschoben (Einfügung) [9]
- hat nach oben verschoben [9]: (Essery et al., 2009; Rutter et al., 2009)
- hat gelöscht: -
- hat gelöscht: January
- Feldfunktion geändert

1021 an international intercomparison project to evaluate twenty-seven current snow models against local and global
1022 observations for a wide variety of settings, including snow schemes that are included in Earth System Models
1023 (Krinner et al., 2018). A further objective of ESM-SnowMIP is to better quantify snow-related feedbacks in the
1024 Earth system. ESM-SnowMIP is tightly linked to the Land Surface, Snow and Soil Moisture Model
1025 Intercomparison Project (<https://climate-cryosphere.org/ls3mip/>; last access: June 1, 2024), which is a contribution
1026 to the 6th phase of the Coupled Model Intercomparison Project (CMIP6; <https://wcrp-cmip.org/cmip-phase-6-cmip6/>;
1027 last access: June 1, 2024). One of the results of ESM-SnowMIP was an unexpected surprise: more sites,
1028 more years and more variables do not necessarily provide more insight into key snow processes; instead, "this led
1029 to the same conclusions as previous MIPs: albedo is still a major source of uncertainty, surface exchange
1030 parameterizations are still problematic, and individual model performance is inconsistent. In fact, models are less
1031 classifiable with results from more sites, years and evaluation variables" (Menard et al., 2021). Currently,
1032 openAMUNDSSEN belongs to the range of models within the COPE initiative (Common Observing Period
1033 Experiment) of the INARCH project (<https://inarch.usask.ca/science-basins/cope.php>;
1034 last access: June 1, 2024). It can be expected that many new insights about the models internals will mutually be learned from these model
1035 intercomparisons in the upcoming future.

1036 6 Conclusions

1037 In this paper, we present openAMUNDSSEN, a fully distributed open source snow-hydrological model for
1038 mountain catchments. The model includes a wide range of process representations of empirical, semi-empirical
1039 and physical nature. openAMUNDSSEN allows to find a compromise between temporal and spatial resolution, time
1040 span of the simulation experiment, size of the considered region, physical detail and consistency as well as
1041 performance. E.g., it offers to choose between the temperature index approach to determine snowmelt rates from
1042 daily temperature and precipitation, or hourly closure of the surface energy balance and calculation of a number
1043 of state variables for several snow layers using temperature, precipitation, humidity, radiation and wind speed as
1044 forcing data. openAMUNDSSEN is computationally efficient, of modular nature, easily extendible and also allows
1045 for using factorial designs to determine interactions between processes and their effect on the accuracy of the
1046 simulation results (Essery et al., 2013; Günther et al., 2019, 2020). Hence, the application of the model is very
1047 flexible and it supports a multitude of applications or simulation experiments to address any kind of hydrological,
1048 glaciological, climatological or related research questions.

1049 The model has been evaluated and proven its applicability at many sites worldwide. Most of all, it was subject to
1050 a systematic, innovative, multilevel spatiotemporal validation with independent datasets of various resolution and
1051 extent from an instrumented site in the European Alps (Hanzer et al., 2016). In all cases, the model showed high
1052 overall skill and well captured the spatial and temporal patterns as well as magnitudes of the observations.

1053 The Python model code for openAMUNDSSEN is available for the public as open source project on GitHub
1054 (<https://github.com/openamundsen/openamundsen>; last access: June 1, 2024), including a documentation which is
1055 subject to continuous extension and improvement (<https://doc.openamundsen.org>; last access: June 1, 2024). The
1056 bootstrap resampling weather generator (see Appendix) is available at
1057 <https://github.com/openamundsen/openamundsen-climategenerator>, (last access: June 1, 2024).

1058 7 Future developments

1059 The openAMUNDSSEN model code is continuously further improved and extended. The modelling of the
1060 processes of lateral snow redistribution will benefit from a simulation of local wind fields, e.g. as recently
1061 demonstrated by Quéno et al. (2023). On top of the wind-induced processes of saltation, turbulent suspension (with
1062 sublimation) snow is also transported downslope by means of avalanches, the origin also of accumulated masses
1063 of snow leewards of crests. In the original, IDL-based version of AMUNDSSEN (Strasser, 2008) the avalanche
1064 process has been parameterized based on the Mflow-TD algorithm by Gruber (2007); the latter was later extended
1065 with a continuous update of the surface elevation model to correct for eroded/deposited masses of snow (Bernhardt
1066 and Schulz, 2010). A comparable algorithm is in development to be included in openAMUNDSSEN soon. Another
1067 path of improvement is foreseen for the snow-canopy interaction module. On the one hand, the parameterization
1068 of inside-canopy meteorological variables derived from measurements taken in the open will be further improved
1069 by utilizing the new (winter) measurements of inside-canopy meteorological variables, i.e. from the Col de Porte
1070 meteorological station in the French Alps (Sicart et al., 2023). Further, it is intended to couple the snow-canopy
1071 interaction module with a dynamically simulated evolution of the LAI from iLand model simulations (Seidl et al.,
1072 2012). The ultimate goal of this effort is to bi-directionally couple the snow processes inside the canopy with its
1073 long-term evolution to enable the simulation of scenarios of the effect of climate change on the coupled
1074 hydrological/biological system of mountain forests.

hat gelöscht: January

Feldfunktion geändert

Feldfunktion geändert

hat gelöscht: January

hat gelöscht: observation

hat gelöscht: period

hat gelöscht: experiment

hat gelöscht: s

hat gelöscht: January

Feldfunktion geändert

hat gelöscht: fold

hat gelöscht: near

hat gelöscht: 7

hat gelöscht: January

Feldfunktion geändert

hat gelöscht: January

Feldfunktion geändert

hat gelöscht: climate

hat gelöscht: (last access: January 1, 2024).

hat formatiert: Schriftfarbe: Text 1

hat gelöscht: 8

hat gelöscht: s

1091 To compute streamflow discharge in mostly glacierized catchment to be compared to gauge recordings, a linear
1092 reservoir cascade approach following Asztalos (2007) has been implemented as a separate post-processing tool
1093 (Hanzer et al., 2016). The linear reservoir approach is a comparable simple empirical method to produce a runoff
1094 curve for a certain location of the stream without the need to provide physical parameters for the catchment
1095 characteristics (e.g., soil), or the wave propagation along the channel. Instead, a series of parallel linear reservoir
1096 cascades (Nash, 1960) is computed the parameters of which are calibrated by maximizing the Nash-Sutcliffe
1097 efficiency NSE and minimizing the relative volume error (following Lindström, 1997). Due to its purely empirical
1098 nature and the fact that its application is limited to small glacierized catchments with short concentration time
1099 only, the linear reservoir approach will not be included into the openAMUNDSEN project on the
1100 openAMUNDSEN GitHub repository. Instead, it is foreseen to test and develop new approaches in machine
1101 learning, e.g. in the field of LSTM (Long Short-Term Memory Networks Modelling) which can provide very good
1102 results for hydrological streamflow simulations (Kratzert et al., 2021). Other such new developments also exist in
1103 the combination of hydrological modelling, remote sensing and machine learning (De Gregorio et al., 2019a and
1104 b). Since AI is a field of rapid development in scientific modelling we expect significant advances also in snow-
1105 hydrological modelling using these innovative methods.

hat gelöscht: promising

1106 Finally, we see a promising way to increase the model accuracy by assimilating satellite data derived maps of,
1107 e.g., snow coverage and/or wet snow area to select the best matching model run out of an ensemble of simulations
1108 that has been created by perturbing the meteorological forcing or the parameters of the model. First developments
1109 are already undertaken in this direction. This way the model can also be accurately initialized when applied for
1110 predictions using weather forecast model output as meteorological forcing.

1111 Appendix: Generation of potential future climate in openAMUNDSEN

1112 Data timeseries of future climate evolution to force openAMUNDSEN for climate change scenario simulations
1113 can be produced by means of a stochastic block bootstrap resampler which is realized as external pre-processing
1114 routine (<https://github.com/openamundsen/openamundsen-climategenerator>; last access June 1, 2024). The
1115 method requires a sufficiently long time series of historical meteorological recordings from a period with as much
1116 as possible variable weather conditions in the considered region. The principles of the implemented weather
1117 generator follow Strasser (2008) and are described herein. Basic assumption of the method is that a climate
1118 storyline can be divided into time periods which are characterized by a certain mean temperature and precipitation
1119 and that these two variables are not independent from each other.

$$1120 \quad P_{\text{tot}} = f(T_{\text{mean}})$$

1121 Thereby P_{tot} is the total precipitation amount of a specific time period, T_{mean} is the mean temperature and f their
1122 functional dependency. The time periods can be set to any length, i.e. to months as in Mauser et al. (2007) or to
1123 weeks as in Strasser (2008). In a first step, the typical annual course of the measured meteorological variables is
1124 constructed by computing mean temperature and total precipitation for the periods using all years of the historical
1125 dataset and applying the given formula. Whereas temperature is characterized by a typical seasonal course in the
1126 Alpine region (warm in summer, cold in winter), the annual course of the precipitation totals of a period with
1127 certain duration can be more complex. The resulting mean annual climate course is used to construct the future
1128 data time series period by period: firstly, the respective temperature for the period is modified with a random
1129 variation factor and an assumed projected temporal trend (e.g., as derived from a regional climate model
1130 application). Then a corresponding precipitation is derived and, again, a random variation. In the end the climate
1131 of a future period is defined by the so obtained mean temperature and precipitation. In a final step, the period from
1132 the historical pool having the most similar temperature and precipitation is selected by applying an Euclidian
1133 nearest neighbour distance measure. All respective data of the chosen period (e.g., air temperature, precipitation,
1134 global radiation, relative humidity and wind speed) are then added to the future time series to be constructed. This
1135 procedure is continuously repeated for all periods of the year, and for all years of the future time series. By
1136 modifying the applied random variation a change in climate variability can be simulated. To allow for more
1137 flexibility in the construction of the periods, in our implementation the basic population from which the measured
1138 period is chosen (= the number of periods available, being equal to the number of years for which observational
1139 data is available) can be synthetically extended by allowing for one or more periods before and after the one to be
1140 constructed (figure A1).

hat gelöscht: suggested

hat gelöscht: ,

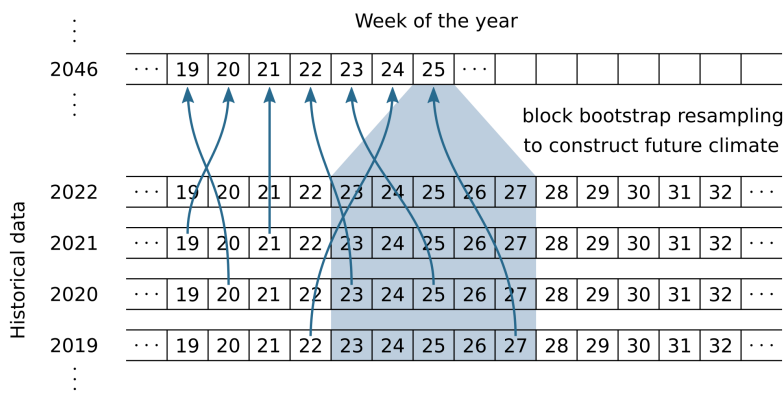


Figure A1: openAMUNDSSEN pre-processing with the weather generator: choice of corresponding historical periods to construct a data timeseries of future climate evolution with preset trend and random variation from given meteorological observations. The number of periods from which data can be selected to construct a particular period of a year in the future time series is set to five in this example.

The described procedure has a number of specific features: (i) the key advantage of the method is that the physical relationship between the meteorological variables is maintained in the simulation; (ii) bootstrap models, such as the described one, obviously work well at high temporal resolution, e.g. 1 to 3-hourly; (iii) the produced data time series is in the validated range for the subsequent hydrological modelling; (iv) a synthetic baseline scenario can easily be constructed by assuming a zero trend for temperature; (v) the procedure is computationally very efficient and finally, (vii) the spatial resolution of the data is preserved as it exactly corresponds to the weather station locations. However, a significant drawback of the method is that auto-correlation between the periods is lost and the consideration of changes in the variability of the meteorological variables is limited. Together with the fact that changes in extreme values are not considered (only their frequency can change) it becomes clear that the data resulting from the method cannot be used for modelling variations in the extent of hydrological extremes. Furthermore and most crucial, no coupling is considered between the (simulated) characteristics of the land surface – e.g. whether it is snow-covered or not – and the atmosphere, and therefore the important effects of feedback mechanisms are not conserved in the construction of the data timeseries. This, however, is a drawback that also many physical climate models share. Examples of the application of the procedure to the high Alpine region of the Berchtesgaden Alps (Germany) with subsequent modelling of snow processes, including snow-canopy interaction, are given in Strasser (2008).

Code availability.

The openAMUNDSSEN model code is available under the MIT license, a short and simple permissive license with conditions only requiring preservation of copyright and license notices. The download site for the model code is <https://github.com/openamundsen/openamundsen> (last access: June 1, 2024). The model in the presented version v1.0 is available on Zenodo (Hanzer et al., 2024).

Data availability.

We provide a comprehensive data set that can be used with openAMUNDSSEN for the high alpine research catchment of the upper Rofenache (98.1 km², Ötztal Alps, Tyrol/Austria) under the Creative Commons Attribution License at PANGAEA (<https://doi.org/10.1594/PANGAEA.876120>; last access: June 1, 2024) including (i) glaciological data, i.e., recordings of glacier volume and geometry changes; (ii) meteorological data as recorded by temporally installed or permanent automatic weather stations; (iii) hydrological data characterizing the water balance of the respective glaciated (sub-) catchment; and (iv) airborne and terrestrial laser scanning data (Strasser et al. 2018). The data time series cover periods of various lengths until 2017. This data is currently extended until August 2023 under the same license (Warscher et al., 2024) and available at <https://doi.org/10.5880/fidgeo.2023.037> (not active yet; temporarily it is <https://dataservices.gfz-potsdam.de/panmetaworks/review/3671ef380a6c433e48f5ec5a4cfa1179dd88c1af297665405aaa139e7b77c24a/>; last access: June 1, 2024).

- hat gelöscht: January
- Feldfunktion geändert
- hat gelöscht: 0.8.3
- hat gelöscht: <https://zenodo.org/records/10462109> (last access: January 6, 2024)
- hat gelöscht: January
- Feldfunktion geändert
- Feldfunktion geändert
- Feldfunktion geändert
- hat gelöscht: January

1188 *Sample availability.*

1189 The sample data for the Rofental research catchment (Ötztal Alps, Austria) which has been used to produce the
1190 figures is available at <https://doi.org/10.1594/PANGAEA.876120> (last access: June 1, 2024) and at
1191 <https://doi.org/10.5880/figgeo.2023.037> (not active yet; temporarily it is [https://dataservices.gfz-](https://dataservices.gfz-potsdam.de/panmetaworks/review/3671cf380a6c433e48f5ec5a4cfa1179dd88c1af297665405aaa139e7b77c24a/)
1192 [potsdam.de/panmetaworks/review/3671cf380a6c433e48f5ec5a4cfa1179dd88c1af297665405aaa139e7b77c24a/](https://dataservices.gfz-potsdam.de/panmetaworks/review/3671cf380a6c433e48f5ec5a4cfa1179dd88c1af297665405aaa139e7b77c24a/);
1193 last access: June 1, 2024. See also Warscher et al., 2024). Further, an openAMUNDSEN setup is available at
1194 <https://github.com/openamundsen/openamundsen-examples> (last access: June 1, 2024).

1195 *Author contributions.*

1196 US designed and developed the original version of the AMUNDSEN model and wrote the paper manuscript; MW
1197 did many model experiments, wrote the documentation, further develops the model, processes the Rofental data,
1198 supports the maintenance of the GitHub site and contributed to the final version of the manuscript; ER supported
1199 the example application model simulations and the manuscript writing process, produced the figures and
1200 contributes to further model development; FH developed many parts of the model in the IDL version, designed
1201 and implemented the new Python version, continuously further develops the model, supervises the GitHub
1202 repository and any improvement there as well as wrote the technical parts of the manuscript of this paper.

1203 *Competing interests.*

1204 The authors declare that no competing interests exist.

1205 *Disclaimer.*

1206 TEXT

1207 *Acknowledgements.*

1208 Since the beginning of the AMUNDSEN model development, many colleagues have contributed with their
1209 valuable experience in field work, modelling and programming. In the early days, the basics for the general design
1210 of such a model were learned from Wolfram Mauser (University of Munich, Germany), and in particular for
1211 anything snow-specific from “Wasti” Markus Weber, Heidi Escher-Vetter and Ludwig Braun (Bavarian Academy
1212 of Sciences Munich, Germany) as well as from Michael Kuhn (University of Innsbruck, Austria). Later, the model
1213 code was further developed using the valuable experiences from a 1-year-position of visiting scientist at the Centre
1214 d’Etudes de la Neige CEN in Grenoble, France. There, the model mostly profited from the lessons learned from
1215 Yves Lejeune, Pierre Etchevers † and Eric Martin, as well as from the other colleagues of the crew at the snow
1216 research center in 1999/2000. At CEN, the first author learned a lot about snow processes and their modelling
1217 from first hand of the professionals. The Arolla glacier expedition 2001, with a lot of joint learning success, was
1218 supported by Paolo Burlando, Francesca Pellicciotti and Martin Funk (all ETH Zurich), Javier Corripio (University
1219 of Edinburgh, Scotland) and Ben Brock (University of Dundee, Scotland). Ongoing testing, improvements as well
1220 as support for further model development in several projects and publications was contributed by Monika Prasch
1221 and Matthias Bernhardt (both University of Munich, Germany) as well as Thomas Marke (University of Innsbruck,
1222 Austria). The model development also significantly profited from the support of the Berchtesgaden National Park
1223 administration, namely Michael Vogel, Helmut Franz and Annette Lotz (Berchtesgaden, Germany). Many field
1224 work experiences by Stefan Pohl † and Jakob Garvelmann helped to improve the process descriptions for the forest
1225 canopy module. In general, by many provided opportunities in joint projects, the openAMUNDSEN model
1226 development generally profited from the work of Samuel Morin (Meteo-France, Grenoble, France), Richard
1227 Essery (University of Edinburgh, Scotland), Glen E. Liston (Cooperative Institute for Research in the
1228 Atmosphere/Fort Collins, Colorado) and John Pomeroy (University of Saskatchewan, Canada). The satellite data
1229 was processed and provided by Thomas Nagler and Gabriele Schwaizer (Enveo, Innsbruck) in the framework of
1230 the AlpSnow project. The LTSER platform Tyrolean Alps – which the Rofental site belongs to – is part of the
1231 national and international long term ecological research network LTER-Austria, LTER Europe and ILTER. This
1232 infrastructure is financially supported by the University of Innsbruck (Faculty of Geo- and Atmospheric Sciences);
1233 it is part of its Research Area “Mountain Regions”. The University of Innsbruck generously supported the complete
1234 re-design and programming of the model in Python and hence the possibility to provide it as open source code to
1235 the scientific community. Finally, the University of Innsbruck also gratefully supported the open access
1236 publication of this paper. Last, but not least, we gratefully acknowledge the valuable review work provided by
1237 Richard Essery and an anonymous reviewer.

hat gelöscht: January

Feldfunktion geändert

hat gelöscht: ,

hat gelöscht: as well as in form of

hat gelöscht: on

hat gelöscht: January

Feldfunktion geändert

hat gelöscht: ¶

1244 References

1245 Allen, R. G., Pereira, L. S., Raes, D. and Smith, M.: Crop evapotranspiration - Guidelines for computing crop
 1246 water requirements. FAO Irrigation and Drainage Paper No. 56, 174 p. ISBN 92-5-104219-5,
 1247 <https://www.fao.org/3/x0490e/x0490e00.htm>, 1998.

hat gelöscht: FAO 1998, 174 p.

1248 Anderson, E. A.: A point energy and mass balance model of a snow cover. NOAA Technical Report NWS 19, pp.
 1249 1–172, <https://repository.library.noaa.gov/view/noaa/6392>, 1976.

hat gelöscht: (

hat gelöscht:).

hat gelöscht: NOAA,

1250 Asztalos, J., Kirnbauer, R., Escher-Vetter, H. and Braun, L.: A distributed energy balance snowmelt model as a
 1251 component of a flood forecasting system for the Inn river. In: Strasser, U. and Vogel M. (eds.) (2008): Proceedings
 1252 of the Alpine*Snow*Workshop, Munich, October 5–6, 2006, Germany. Research report 53, ISBN13 978-3-
 1253 922325-60-4, National Park Berchtesgaden, 2007.

1254 [Barnes, S. L.: A technique for maximising details in numerical weather map analysis. J. Appl. Meteor., 3, pp. 396–
 1255 409, 1964.](#)

1256 [Barnett, T. P., Adam, J. C. and Lettenmaier, D. P.: Potential impacts of a warming climate on water availability in
 1257 snow- dominated regions. Nature, 438, pp. 303–309, <https://doi.org/10.1038/nature04141>, 2015.](#)

hat formatiert: Englisch (USA)

hat formatiert: Englisch (USA)

hat formatiert: Englisch (USA)

hat formatiert: Englisch (USA)

1258 Bavay, M. and Egger, T.: MeteorIO 2.4.2: a preprocessing library for meteorological data. Geosci. Model. Dev.
 1259 Vol. 8, pp. 3135–3151, <https://doi.org/10.5194/gmd-7-3135-2014>, 2014.

1260 Bernhardt, M. and Schulz, K.: SnowSlide: A simple routine for calculating gravitational snow transport. Geophys.
 1261 Res. Lett., Vol. 37, L11 502, <https://doi.org/10.1029/2010GL043086>, 2010.

1262 Blöschl, G.: Scaling issues in snow hydrology. Hydrol. Process., Vol. 13, pp. 2149–2175, 1999.

hat gelöscht: :

1263 Blöschl, G. and Kirnbauer, R.: Point snowmelt models with different degrees of complexity–internal processes. J.
 1264 Hydrol., Vol. 129, pp. 127–147, [https://doi.org/10.1016/0022-1694\(91\)90048-M](https://doi.org/10.1016/0022-1694(91)90048-M), 1991.

1265 Braun, L. N.: Simulation of snowmelt-runoff in lowland and lower alpine regions of Switzerland. Ph.D. thesis,
 1266 ETH Zurich, 1984.

1267 Corripio, J.: Vectorial algebra algorithms for calculating terrain parameters from DEMs and solar radiation
 1268 modelling in mountainous terrain. Int. J. Geogr. Inf. Sci., Vol. 17(1), pp. 1–23, <https://doi.org/10.1080/713811744>,
 1269 2003.

hat gelöscht: -

1270 De Gregorio, L., Günther, D., Callegari, M., Strasser, U., Zebisch, M., Bruzzone, L. and Notarnicola, C.:
 1271 Improving SWE Estimation by Fusion of Snow Models with Topographic and Remotely Sensed Data. Rem. Sens.,
 1272 11(17), 2033, <https://doi.org/10.3390/rs11172033>, 2019a.

1273 De Gregorio, L., Callegari, M., Marin, C., Zebisch, M., Bruzzone, L., Demir, B., Strasser, U., Marke, T., Günther,
 1274 D., Nadalet, R. and Notarnicola, C.: A novel data fusion technique for snow cover retrieval. J. Sel. Top. Appl.
 1275 Earth Obs. Rem. Sens. JSTARS, Vol. 12, No. 8, <https://doi.org/10.1109/JSTARS.2019.2920676>, 2019b.

1276 Ebner, P. P., Koch, F., Premier, V., Marin, C., Hanzer, F., Carmagnola, C. M., Hugues, F., Günther, D., Monti, F.,
 1277 Hargoa, O., Strasser, U., Morin, S. and Lehning, M.: Evaluating a prediction system for snow management. The
 1278 Cryosphere, <https://doi.org/10.5194/tc-15-3949-2021>, 2021.

1279 [Essery, R., Rutter, N., Pomeroy, J., Baxter, R., Staehli, M., Gustafsson, D., Barr, A., Bartlett, P. and Elder, K.:
 1280 SNOWMIP2: An evaluation of forest snow process simulations. Bull. Am. Met. Soc., 90 \(8\), pp. 1120–1136,
 1281 <https://doi.org/10.1175/2009BAMS2629.1>, 2009.](#)

hat verschoben (Einfügung) [6]

1282 [Essery, R., Morin, S., Lejeune, Y. and Ménard C. B.: A comparison of 1701 snow models using observations from
 1283 an alpine site. Adv. Wat. Res. 55, pp.131–148, <https://doi.org/10.1016/j.advwatres.2012.07.013>, 2013.](#)

Formatiert: Standard (Web)

hat formatiert: Schriftart: (Standard) Times New Roman, Englisch (USA)

1290 [Essery, R.: A factorial snowpack model \(FSM 1.0\). Geosci. Model. Dev. 8, pp. 3867–3876, https://doi.org/10.5194/gmd-8-3867-2015, 2015.](https://doi.org/10.5194/gmd-8-3867-2015)
1291

1292 [Etchevers, P., Martin, E., Brown, R., Fierz, C., Lejeune, Y., Bazile, E., Boone, A., Dai, Y.-J., Essery, R. L. E.,
1293 Fernandez, Y., Gusev, Y., Jordan, R., Foren, V., Kowalczyk, E., Nasonova, N. O., Pyles, R. D., Schlosser, A.,
1294 Shmakin, A. B., Smirnova, T. G., Strasser, U., Verseghy, D., Yamazaki, T. and Yang, Z.-L.: Validation of the
1295 surface energy budget simulated by several snow models \(SnowMIP project\). Ann. Glaciol., Vol. 38, pp. 150–
1296 158, https://doi.org/10.3189/172756404781814825, 2004.](https://doi.org/10.3189/172756404781814825)

1297 [Fischer, A., Seiser, B., Stocker-Waldhuber, M., Mitterer, C. and Abermann, J.: Tracing glacier changes in Austria
1298 from the Little Ice Age to the present using a lidar-based high-resolution glacier inventory in Austria. The
1299 Cryosphere, 9\(2\), pp. 753–766, https://doi.org/10.5194/tc-9-753-2015, 2015.](https://doi.org/10.5194/tc-9-753-2015)

1300 Förster, K., Hanzer, F., Winter, B., Marke, T. and Strasser, U.: MELODIST – An open-source Meteorological
1301 observation time series Disaggregation Tool. Geosci. Model Dev., Vol. 9, pp. 2315–2333,
1302 https://doi.org/10.5194/gmd-9-2315-2016, 2016.

1303 [Freudiger, D., Kohn, I., Seibert, J., Stahl, K. and Weiler, M.: Snow redistribution for the hydrological modeling
1304 of alpine catchments. WIREs Water, e1232, pp. 1–16, https://doi.org/10.1002/wat2.1232, 2017.](https://doi.org/10.1002/wat2.1232)

1305 Goodison, B. E., Louie, P., and Yang, D.: WMO solid precipitation measurement intercomparison. Tech. Rep.
1306 WMO/TD 872, Geneva, 1998.

1307 Gruber, S.: A mass-conserving fast algorithm to parameterize gravitational transport and deposition using digital
1308 elevation models. Water Resour. Res., Vol. 43, W06412, https://doi.org/10.1029/2006WR004868, 2007.

1309 [Grünewald, T., Stötter, J., Pomeroy, J. W., Dadic, R., Moreno Baños, I., Marturià, J., Spross, M., Hopkinson, C.,
1310 Burlando, P. and Lehning, M.: Statistical modelling of the snow depth distribution in open alpine terrain. Hydrol.
1311 Earth Syst. Sci., Vol. 17, pp. 3005–3021, https://doi.org/10.5194/hess-17-3005-2013, 2013.](https://doi.org/10.5194/hess-17-3005-2013)

1312 Grünewald, T., Bühler, Y. and Lehning, M.: Elevation dependency of mountain snow depth. The Cryosphere, 8,
1313 pp. 2381–2394, https://doi.org/10.5194/tc-8-2381-2014, 2014.

1314 [Günther, D., Marke, T., Essery, R. and Strasser, U.: Uncertainties in Snowpack Simulations – Assessing the Impact
1315 of Model Structure, Parameter and Forcing Data Error on Point-Scale Energy-Balance Snow Model Performance.
1316 Water Resour. Res., Vol. 55, pp. 2779–2800, https://doi.org/10.1029/2018WR023403, 2019.](https://doi.org/10.1029/2018WR023403)

1317 Günther, D., Hanzer, F., Warscher, M., Essery, R. and Strasser, U.: Including parameter uncertainty in an
1318 intercomparison of physically-based snow models. Front. Earth Sci., Vol. 8, 542599,
1319 https://doi.org/10.3389/feart.2020.542599, 2020.

1320 Hanzer, F., Marke, T. and Strasser, U.: Distributed, explicit modelling of technical snow production for a ski area
1321 in the Schladming Region (Austrian Alps). Cold Reg. Sci. Technol., Vol. 108, pp. 113–124,
1322 https://doi.org/10.1016/j.coldregions.2014.08.003, 2014.

1323 Hanzer, F., Helfricht, K., Marke, T. and Strasser, U.: Multi-level spatiotemporal validation of snow/ice mass
1324 balance and runoff modeling in glacierized catchments. The Cryosphere, Vol. 10, pp. 1859–1881,
1325 https://doi.org/10.5194/tc-10-1859-2016, 2016.

1326 Hanzer, F., Förster, K., Nemeč, J. and Strasser, U.: Projected hydrological and cryospheric impacts of 21st century
1327 climate change in the Ötztal Alps (Austria) simulated using a physically based approach. Hydrol. Earth Syst. Sci.,
1328 Vol. 22, pp. 1593–1614, https://dx.doi.org/10.5194/hess-22-1593-2018, 2018.

1329 Hanzer, F., Carmagnola, C. M., Ebner, P. P., Koch, F., Monti, F., Bavay, M., Bernhardt, M., Lafaysse, M.,
1330 Lehning, M., Strasser, U., François, H. and Morin, S.: Simulation of snow management in Alpine ski resorts using
1331 three different snow models. Cold Reg. Sci. Technol., Vol. 172, 102995,
1332 https://doi.org/10.1016/j.coldregions.2020.102995, 2020.

hat verschoben (Einfügung) [4]

hat nach unten verschoben [5]: Fischer, A., Seiser, B., Stocker-Waldhuber, M., Mitterer, C. and Abermann, J.: Tracing glacier changes in Austria from the Little Ice Age to the present using a lidar-based high-resolution glacier inventory in Austria. The Cryosphere, 9(2), pp. 753–766, https://doi.org/10.5194/tc-9-753-2015, 2015.

hat nach oben verschoben [4]: Essery, R.: A factorial snowpack model (FSM 1.0). Geosci. Model. Dev. 8, pp. 3867–3876, https://doi.org/10.5194/gmd-8-3867-2015, 2015.

hat nach oben verschoben [6]: Essery, R., Rutter, N., Pomeroy, J., Baxter, R., Staehli, M., Gustafsson, D., Barr, A., Bartlett, P. and Elder, K.: SNOWMIP2: An evaluation of forest snow process simulations. Bull. Am. Met. Soc. 90 (8), pp. 1120–1136, https://doi.org/10.1175/2009BAMS2629.1, 2009.

Essery, R., Morin, S., Lejeune, Y. and Ménard C. B.: A comparison of 1701 snow models using observations from an alpine site. Adv. Wat. Res. 55, pp.131–148, 2013.

hat verschoben (Einfügung) [5]

hat formatiert: Englisch (USA)

hat formatiert: Englisch (USA)

hat formatiert: Englisch (USA)

hat formatiert: Absatz-Standardschriftart, Schriftart: 12 Pt., Deutsch

hat formatiert: Englisch (USA)

hat gelöscht: ,

hat verschoben (Einfügung) [7]

hat nach oben verschoben [7]: Grünewald, T., Stötter, J., Pomeroy, J. W., Dadic, R., Moreno Baños, I., Marturià, J., Spross, M., Hopkinson, C., Burlando, P. and Lehning, M.: Statistical modelling of the snow depth distribution in open alpine terrain. Hydrol. Earth Syst. Sci., Vol. 17, pp. 3005–3021, https://doi.org/10.5194/hess-17-3005-2013, 2013.

hat formatiert: Deutsch

1360 [Hanzer, F., Warscher, M. and Strasser, U.: openAMUNDSEN v1.0.0 \(v1.0.0\). Zenodo.](https://doi.org/10.5281/zenodo.11859175)
1361 [https://doi.org/10.5281/zenodo.11859175, 2024.](https://doi.org/10.5281/zenodo.11859175)

1362 Harris, C. R., Millman, K. J., van der Walt, S. J., Gommers, R., Virtanen, P., Cournapeau, D., Wieser, E., Taylor,
1363 J., Berg, S., Smith, N. J., Kern, R., Picus, M., Hoyer, S., van Kerkwijk, M. H., Brett, M., Haldane, A., del Río, J.
1364 F., Wiebe, M., Peterson, P., Gérard-Marchant, P., Sheppard, K., Reddy, T., Weckesser, W., Abbassi, H., Gohlke,
1365 C. and Oliphant, T. E.: Array programming with NumPy. *Nature*, 585(7825), 7825,
1366 <https://doi.org/10.1038/s41586-020-2649-2>, 2020.

1367 Huss, M. and Farinotti, D.: Distributed ice thickness and volume of all glaciers around the globe. *J. Geophys. Res.*
1368 *Earth Surface*, Vol. 117, F04010, <https://doi.org/10.1029/2012JF002523>, 2012.

1369 Helfricht, K.: Analysis of the spatial and temporal variation of seasonal snow accumulation in Alpine catchments
1370 using airborne laser scanning. Ph.D. thesis, Innsbruck, 2014.

1371 Hoyer, S. and Hamman, J.: xarray: N-D labeled Arrays and Datasets in Python. *Journal Open Res. Soft.*, 5(1),
1372 <https://doi.org/10.5334/jors.148>, 2017.

1373 Kochendorfer, J., Rasmussen, R., Wolff, M., Baker, B., Hall, M. E., Meyers, T., Landolt, S., Jachcik, A., Isaksen,
1374 K., Brækkan, R. and Leeper, R.: The quantification and correction of wind-induced precipitation measurement
1375 errors. *Hydrol. Earth Syst. Sci.*, 21(4), pp. 1973–1989, <https://doi.org/10.5194/hess-21-1973-2017>, 2017.

1376 Koivusalo, H., Heikinheimo, M. and Karvonen, T.: Test of a simple two-layer parameterisation to simulate the
1377 energy balance and temperature of a snow pack. *Theor. Appl. Clim.*, 70(1–4), pp. 65–79,
1378 <https://doi.org/10.1007/s007040170006>, 2001.

1379 Kratzert, F., Gauch, M., Nearing, G., Hochreiter, S. and Klotz, D.: Niederschlags-Abfluss-Modellierung mit Long
1380 Short-Term Memory (LSTM). *Österr. Wasser- und Abfallw.*, <https://doi.org/10.1007/s00506-021-00767-z>, 2021.

1381 Krinner, G., Derksen, C., Essery, R., Flanner, M., Hagemann, S., Clark, M., Hall, A., Rott, H., Brutel-Vuilment,
1382 C., Kim, H., Ménard, C., Mudryk, L., Thackeray, C., Arduini, G., Bartlett, P., Boone, A., Chérury, F., Colin, J.,
1383 Cuntz, M., Dai, Y., Decharme, B., Derry, J., Ducharne, A., Dutra, E., Fang, X., Fierz, C., Ghattas, J., Gusev, Y.,
1384 Haverd, V., Kontu, A., Lafaysse, M., Law, R., Lawrence, D., Li, W., Marke, T., Marks, D., Nasonova, O., Nitta,
1385 T., Niwano, M., Pomeroy, J., Raleigh, M. S., Schaedler, G., Semenov, V., Smirnova, T., Stacke, T., Strasser, U.,
1386 Svenson, S., Turkov, D., Wang, L., Wang, T., Wever, N., Yuan, H. and Zhou, W.: ESM-SnowMIP: Assessing
1387 models and quantifying snow-related climate feedbacks. *Geosci. Model Dev.*, pp. 5027–5049,
1388 <https://doi.org/10.5194/gmd-11-5027-2018>, 2018.

1389 Lam, S. K., Pitrou, A. and Seibert, S.: Numba: A llvm-based python jit compiler. *Proceedings of the Second*
1390 *Workshop on the LLVM Compiler Infrastructure in HPC*, pp. 1–6, 2015.

1391 Lam, R., Sanchez-Gonzalez, A., Wilson, M., Wirnsberger, P., Fortunato, M., Alet, F., Ravuri, S., Ewalds, T.,
1392 Eaton-Rosen, Z., Hu, W., Merose, A., Hoyer, S., Holland, G., Vinyals, O., Stott, J., Pritzel, A., Mohamed, S. and
1393 Battaglia, P.: Learning skillfull medium-range global weather forecasting. *Science* 382, pp. 1416–1421,
1394 <https://www.science.org/doi/10.1126/science.adi2336>, 2023.

1395 Lehning, M., Bartelt, P., Brown, B., Russi, T., Stockli, U. and Zimmerli, M.: SNOWPACK model calculations for
1396 avalanche warning based upon a new network of weather and snow stations. *Cold Reg. Sci. Technol.*, Vol. 30, pp.
1397 145–157, [https://doi.org/10.1016/S0165-232X\(99\)00022-1](https://doi.org/10.1016/S0165-232X(99)00022-1), 1999.

1398 Lindström, G.: A Simple Automatic Calibration Routine for the HBV Model. *Nord. Hydrol.*, Vol. 28, pp. 153–
1399 168, [ISSN 0029-1277, E-ISSN 1996-9694](https://doi.org/10.1016/S0165-232X(99)00022-1), 1997.

1400 Liston, G. E. and Elder, K.: A meteorological distribution system for high-resolution terrestrial modeling
1401 (MicroMet). *J. Hydrometeorol.*, 7(2), pp. 217–234, <https://doi.org/10.1175/JHM486.1>, 2006.

hat formatiert: Absatz-Standardschriftart,
Schriftart: 12 Pt.

hat formatiert: Deutsch (Österreich)

hat formatiert: Deutsch

hat formatiert: Deutsch

hat gelöscht: 2023

hat formatiert: Englisch (USA)

1403 [Marke, T.: Development and Application of a Model Interface To couple Land Surface Models with Regional](#)
1404 [Climate Models For Climate Change Risk Assessment In the Upper Danube Watershed. Dissertation, Ludwig-](#)
1405 [Maximilians-Universität München. 188 p., München, <https://doi.org/10.5282/edoc.9162>, 2008.](#)

1406 Marke, T., Strasser, U., Hanzer, F., Wilcke, R., Gobiet, A. and Stötter, J.: Scenarios of future snow conditions in
1407 Styria (Austrian Alps). *J. Hydrometeor.*, Vol. 16, pp. 261–277, <https://doi.org/10.1175/JHM-D-14-0035.1>, 2015.

1408 Marke, T., Mair, E., Förster, K., Hanzer, F., Garvelmann, J., Pohl, S., Warscher, M. and Strasser, U.:
1409 ESCIMO.spread (v2): Parameterization of a spreadsheet-based energy balance snow model for inside-canopy
1410 conditions, *Geosci. Model Dev.*, Vol. 9, pp. 633–646, <https://doi.org/10.5194/gmd-9-633-2016>, 2016.

1411 Marke, T., Hanzer, F., Olefs, M. and Strasser, U.: Simulation of Past Changes in the Austrian Snow Cover 1948–
1412 2009. *J. Hydrometeor.*, Vol. 19, pp. 1529–1545, <https://doi.org/10.1175/JHM-D-17-0245.1>, 2018.

1413 Mauser, W., Prasch, M. and Strasser, U.: Physically based Modelling of Climate Change Impact on Snow Cover
1414 Dynamics in Alpine Regions using a Stochastic Weather Generator. Proceedings of the International Congress on
1415 Modelling and Simulation MODSIM07 2007, Christchurch, New Zealand, 2007.

1416 [McKinney, W.: Data Structures for Statistical Computing in Python. Proceedings of the 9th Python in Science](#)
1417 [Conference, pp. 56–61, <https://doi.org/10.25080/Majora-92bf1922-00a>, 2010.](#)

1418 [Menard, C., Essery, R., Krinner, G., Arduini, G., Bartlett, P., Boone, A., Brutel-Vuilmet, C., Burke, E., Cuntz, M.,](#)
1419 [Dai, Y., Decharme, B., Dutra, E., Fang, L., Fierz, C., Gusev, Y., Hagemann, S., Haverd, V., Kim, H., Lafaysse,](#)
1420 [M., Marke, T., Nasonova, O., Nitta, T., Niwano, M., Pomeroy, J., Schaedler, G., Semenov, V., Smirnova, T.,](#)
1421 [Strasser, U., Swenson, S., Turkov, D., Wever, N. and Yuan, H.: Scientific and human errors in a snow model](#)
1422 [intercomparison. *Bull. Amer. Meteor. Soc.*, <https://doi.org/10.1175/BAMS-D-19-0329.1>, 2021.](#)

1423 Mott, R., Winstral, A., Cluzet, B., Helbig, N., Magnusson, J., Mazzotti, G., Quéno, L., Schirmer, M., Webster, C.
1424 and Jonas, T.: Operational snow-hydrological modeling for Switzerland. *Front. Earth Sci.*, 11:1228158,
1425 <https://doi.org/10.3389/feart.2023.1228158>, 2023.

1426 Nash, J. E.: A unit hydrograph study, with particular reference to British catchments. *Proc. Inst. Civ. Eng.*, Vol.
1427 17, pp. 249–282, 1960.

1428 Ohmura, A.: Physical basis for the temperature-based melt-index method. *J. Appl. Meteor.*, Vol. 40, pp. 753–761,
1429 2001.

1430 Pellicciotti, F., Brock, B., Strasser, U., Burlando, P., Funk, M. and Corripio, J.: An enhanced temperature-index
1431 glacier melt model including shortwave radiation balance: development and testing for Haut Glacier D’Arolla,
1432 Switzerland. *J. Glaciol.*, Vol. 51, Nr. 175, pp. 573–587, <https://doi.org/10.3189/172756505781829124>, 2005.

1433 Pfeiffer, J., Zieher, T., Schmieder, J., Rutzinger, M. and Strasser, U.: Spatio-temporal assessment of the
1434 hydrological drivers of an active deep-seated gravitational slope deformation – the Vögelsberg landslide in Tyrol
1435 (Austria). *Earth Surf. Proc. Landf.*, <http://doi.org/10.1002/esp.5129>, 2021.

1436 Podsiadlo, I., Paris, C., Callegari, M., Marin, C., Günther, D., Strasser, U., Notarnicola, C. and Bruzzone, L.:
1437 Integrating models and remote sensing data for distributed glacier mass balance estimation. *J. Sel. Top. Appl.*
1438 *Earth Obs. Rem. Sens. JSTARS*, Vol. 13, pp. 6177–6194, <https://doi.org/10.1109/JSTARS.2020.3028653>, 2020.

1439 Quéno, L., Mott, R., Morin, P., Cluzet, B., Mazzotti, G. and Jonas, T.: Snow redistribution in an intermediate-
1440 complexity snow hydrology modelling framework. *EGUsphere* [preprint], <https://doi.org/10.5194/egusphere-2023-2071>, 2023.

1442 Rasmussen, R., Baker, B., Kochendorfer, J., Meyers, T., Landolt, S., Fischer, A. P., Black, J., Thériault, J. M.,
1443 Kucera, P., Gochis, D., Smith, C., Nitu, R., Hall, M., Ikeda, K. and Gutman, E.: How well are we measuring snow?
1444 The NOAA/FAA/NCAR Winter Precipitation Test Bed. *Bull. Am. Met. Soc.*, pp. 811–829,
1445 <https://doi.org/10.1175/BAMS-D-11-00052.1>, 2012.

hat formatiert: Englisch (USA)

hat formatiert: Englisch (USA)

hat formatiert: Englisch (USA)

hat formatiert: Deutsch

hat nach unten verschoben [8]: McKinney, W.: Data Structures for Statistical Computing in Python. Proceedings of the 9th Python in Science Conference, pp. 56–61, <https://doi.org/10.25080/Majora-92bf1922-00a>, 2010.

hat gelöscht: <https://doi.org/10.5282/edoc.9162>

hat gelöscht: ,

hat formatiert: Schriftart: 10 Pt.

hat nach unten verschoben [3]: Menard, C., Essery, R., Krinner, G., Arduini, G., Bartlett, P., Boone, A., Brutel-Vuilmet, C., Burke, E., Cuntz, M., Dai, Y., Decharme, B., Dutra, E., Fang, L., Fierz, C., Gusev, Y., Hagemann, S., Haverd, V., Kim, H., Lafaysse, M., Marke, T., Nasonova, O., Nitta, T., Niwano, M., Pomeroy, J., Schaedler, G., Semenov, V., Smirnova, T., Strasser, U., Swenson, S., Turkov, D., Wever, N. and Yuan, H.: Scientific and human errors in a snow model intercomparison. *Bull. Amer. Meteor. Soc.*, <https://doi.org/10.1175/BAMS-D-19-0329.1>, 2021.

hat gelöscht: -

hat verschoben (Einfügung) [8]

hat verschoben (Einfügung) [3]

- 1463 Rohrer, M. B.: Die Schneedecke im schweizerischen Alpenraum und ihre Modellierung. Zürcher Geographische
1464 Schriften, 49, 178, 1992.
- 1465 Rutter, N., Essery, R. L. E., Pomeroy, J., Altimir, N., Andreadis, K., Baker, I., Barr, A., Bartlett, P., Elder, K.,
1466 Ellis, C., Feng, X., Gelfan, A., Goodbody, G., Gusev, Y., Gustafsson, D., Hellström, R., Hirota, T., Jonas, T.,
1467 Koren, V., Li, W.-P., Luce, C., Martin, E., Nasonova, O., Pumpanen, J., Pyles, D., Samuelsson, P., Sandells, M.,
1468 Schädler, G., Shmakin, A., Smirnova, T., Stähli, M., Stöckli, R., Strasser, U., Su, H., Suzuki, K., Takata, K.,
1469 Tanaka, K., Thompson, E., Vesala, T., Viterbo, P., Wiltshire, A., Xue, Y. and Yamazaki, T.: Evaluation of forest
1470 snow processes models (SnowMIP2). *J. Geophys. Res.*, 114, D06111, <https://doi.org/10.1029/2008JD011063>,
1471 2009.
- 1472 Sauter, T., Arndt, A. and Schneider, C.: COSIPY v1.3 – an open-source coupled snowpack and ice surface energy
1473 and mass balance model. *Geosci. Model Dev.*, Vol. 13, pp. 5645–5662, [https://doi.org/10.5194/gmd-13-5645-](https://doi.org/10.5194/gmd-13-5645-2020)
1474 2020, 2020.
- 1475 Seibert, J. and Bergström, S.: A retrospective on hydrological catchment modelling based on half a century with
1476 the HBV model. *Hydrol. Earth Syst. Sci.*, Vol. 26, pp. 1371–1388, <https://doi.org/10.5194/hess-26-1371-2022>,
1477 2022.
- 1478 Seidl, R., Rammer, W., Scheller, R. M. and Spies, T. A.: An individual-based process model to simulate landscape-
1479 scale forest ecosystem dynamics. *Ecol. Mod.*, Vol. 231, <https://doi.org/10.1016/j.ecolmodel.2012.02.015>, 2012.
- 1480 Sicart, J. M., Ramseyer, V., Picard, G., Arnaud, L., Coulaud, K., Freche, G., Soubeyrand, D., Lejeune, Y., Dumont,
1481 M., Gouttevin, I., Le Gac, E., Berger, F., Monnet, J.-M., Borgniet, L., Mermin, E., Rutter, N., Webster, C. and
1482 Essery, R.: Snow accumulation and ablation measurements in a midlatitude mountain coniferous forest (Col de
1483 Porte, France, 1325 m altitude): the Snow Under Forest (SnoUF) field campaign data set. *Earth Syst. Sci. Data*,
1484 Vol. 15, <https://doi.org/10.5194/essd-15-5121-2023>, 2023.
- 1485 Strasser, U. and Mauser, W.: Modelling the Spatial and Temporal Variations of the Water Balance for the Weser
1486 Catchment 1965–1994. *J. Hydrol.*, Vol. 254/1-4, pp. 199–214, [https://doi.org/10.1016/S0022-1694\(01\)00492-9](https://doi.org/10.1016/S0022-1694(01)00492-9),
1487 2001.
- 1488 Strasser, U., Etchevers, P. and Lejeune, Y.: Intercomparison of two Snow Models with Different Complexity
1489 Using Data from an Alpine Site. *Nordic Hydrol.*, 33 (1), pp. 15–26, <https://doi.org/10.2166/nh.2002.0002>, 2002.
- 1490 Strasser, U., Corripio, J., Brock, B., Pellicciotti, F., Burlando, P. and Funk, M. (2004): Spatial and Temporal
1491 Variability of Meteorological Variables at Haut Glacier d’Arolla (Switzerland) During the Ablation Season 2001:
1492 Measurements and Simulations. *J. Geophys. Res.*, Vol. 109, D03103, <https://doi.org/10.1029/2003JD003973>,
1493 2004.
- 1494 Strasser, U.: Die Modellierung der Gebirgsschneedecke im Nationalpark Berchtesgaden. Modelling of the
1495 mountain snow cover in the Berchtesgaden National Park. Berchtesgaden National Park research report, Nr. 55,
1496 ISBN 978-3-922325-62-8, Berchtesgaden, 2008.
- 1497 Strasser, U., Bernhardt, M., Weber, M., Liston, G. E. and Mauser, W.: Is snow sublimation important in the alpine
1498 water balance? *The Cryosphere*, Vol. 2, pp. 53–66, <https://doi.org/10.5194/tc-2-53-2008>, 2008.
- 1499 Strasser, U. and Marke, T.: ESCIMO.spread - a spreadsheet-based point snow surface energy balance model to
1500 calculate hourly snow water equivalent and melt rates for historical and changing climate conditions. *Geosci.*
1501 *Model Dev.*, Vol. 3, pp. 643–652, <https://doi.org/10.5194/gmd-3-643-2010>, 2010.
- 1502 Strasser, U., Warscher, M. and Liston, G. E.: Modelling snow-canopy processes on an idealized mountain. *J.*
1503 *Hydrometeor.* Vol. 12, No. 4, pp. 663–677, <https://doi.org/10.1175/2011JHM1344.1>, 2011.
- 1504 Strasser, U., Marke, T., Braun, L., Escher-Vetter, H., Juen, I., Kuhn, M., Maussion, F., Mayer, C., Nicholson, L.,
1505 Niederscheider, K., Sailer, R., Stötter, J., Weber, M. and Kaser, G.: The Rofental: a high Alpine research basin
1506 (1890–3770 m a.s.l.) in the Ötztal Alps (Austria) with over 150 years of hydrometeorological and glaciological
1507 observations. *Earth Syst. Sci. Data*, Vol. 10, pp. 151–171, <https://doi.org/10.5194/essd-10-151-2018>, 2018.

hat gelöscht: N

hat gelöscht: -

1510 [Vionnet, V., Brun, E., Morin, S., Boone, A., Faroux, S., Le Moigne, P., Martin, E. and Willemet, J.-M.: The](#)
1511 [detailed snowpack scheme Crocus and its implementation in SURFEX v7.2. Geosci. Model Dev., Vol. 5, pp. 773–](#)
1512 [791, <https://doi.org/10.5194/gmd-5-773-2012>, 2012.](#)

1513 [Vionnet, V., Marsh, C. B., Menounos, B., Gascoïn, S., Wayand, N., Shea, J., Mukherjee, K. and Pomeroy, J.:](#)
1514 [Multi-scale snowdrift-permitting modelling of mountain snowpack. The Cryosphere, Vol. 15, pp. 743–769,](#)
1515 <https://doi.org/10.5194/tc-15-743-2021>, 2021.

1516 [Vionnet, V., Verville, M., Fortin, V., Brugman, M., Abrahamowicz, M., Lemay, F., Thériault, M., Lafaysse, T.](#)
1517 [and Milbrandt, J.-A.: Snow level from post-processing of atmospheric model improves snowfall estimate and](#)
1518 [snowpack prediction in mountains. Water Resour. Res., Vol. 58, e2021WR031778,](#)
1519 <https://doi.org/10.1029/2021WR031778>, 2022.

1520 [Viviroli, D., Dürr, H. H., Messerli, B., Meybeck, M. and Weingartner, R.: Mountains of the world, water towers](#)
1521 [for humanity: Typology, mapping, and global significance. Water Resour. Res., 43 \(7\),](#)
1522 <https://doi.org/10.1029/2006wr005653>, 2007.

1523 [Viviroli, D., Kummu, M., Meybeck, M., Kallio, M. and Wada, Y.: Increasing dependence of lowland populations](#)
1524 [on mountain water resources. Nature Sustainability, Nature Publishing Group, 3\(11\), pp. 917–928,](#)
1525 <https://doi.org/10.1038/s41893-020-0559-9>, 2020.

1526 [Warscher, M., Strasser, U., Kraller, G., Marke, T., Franz, H. and Kunstmann, H.: Performance of complex snow](#)
1527 [cover descriptions in a distributed hydrological model system: A case study for the high Alpine terrain of the](#)
1528 [Berchtesgaden Alps. Water Resour. Res., Vol. 49, pp. 2619–2637, <https://doi.org/10.1002/wrcr.20219>, 2013.](#)

1529 [Warscher, M., Marke, T., Rottler, E. and Strasser, U.: Operational and experimental snow observation systems in](#)
1530 [the upper Rofental: data from 2017 to 2023. Earth Syst. Sci. Data Discuss. EGU sphere \[preprint\],](#)
1531 <https://doi.org/10.5194/essd-2024-45>, 2024.

1532 [Weber, M.: A parameterization for the turbulent fluxes over melting surfaces derived from eddy correlation](#)
1533 [measurements. In: Strasser, U. and Vogel M. \(eds.\) \(2008\): Proceedings of the Alpine*Snow*Workshop, Munich,](#)
1534 [October 5–6, 2006, Germany. Berchtesgaden National Park research report 53, ISBN13 978-3-922325-60-4,](#)
1535 [Berchtesgaden, 2008.](#)

1536 [Yokoyama, R., Shirasawa, M. and Pike, R. J.: Visualizing topography by openness: a new application of image](#)
1537 [processing to digital elevation models. Photogr. Eng. Rem. Sens., Vol. 68, pp. 257–266, 2002.](#)

hat nach unten verschoben [2]: Weber, M.: A parameterization for the turbulent fluxes over melting surfaces derived from eddy correlation measurements. In: Strasser, U. and Vogel M. (eds.) (2008): Proceedings of the Alpine*Snow*Workshop, Munich, October 5–6, 2006, Germany. Berchtesgaden National Park research report 53, ISBN13 978-3-922325-60-4, Berchtesgaden, 2008.

hat gelöscht: Warscher, M., Marke, T., Rottler, E. and Strasser, U.: Operational and experimental snow observation systems in the upper Rofental: data from 2017–2023. Earth Syst. Sci. Data (in preparation), 2024.

hat formatiert: Schriftart: Nicht Kursiv

hat formatiert: Schriftart: Nicht Kursiv

hat formatiert: Schriftart: Nicht Kursiv, Englisch (USA)

hat formatiert: Absatz-Standardschriftart, Schriftart: 12 Pt., Deutsch

hat formatiert: Schriftart: Nicht Kursiv, Englisch (USA)

hat formatiert: Schriftart: Nicht Kursiv

hat verschoben (Einfügung) [2]

Formatiert: Standard (Web), Block

hat formatiert: Schriftart: 10 Pt.

Seite 10: [1] hat gelöscht

Ulrich Strasser

02.06.24 15:02:00



Seite 14: [2] hat gelöscht

Ulrich Strasser

01.06.24 13:49:00

